

# Practical Treatment of Singlet Oxygen with Density-Functional Theory and the Multiplet-Sum Method

Abraham Ponra

*University of Maroua, Cameroon*

*e-mail: abraaponra@yahoo.com*

Anne Justine Etindele

*Higher Teachers Training College, University of Yaounde I, P.O. Box 47, Yaounde, Cameroon*

*e-mail: annetindele@yahoo.fr*

Ousmanou Motapon

*University of Maroua, Cameroon*

*e-mail: omotapon@univ-douala.com*

Mark E. Casida

*Laboratoire de Spectrométrie, Interactions et Chimie théorique (SITh), Département de Chimie Moléculaire (DCM, UMR CNRS/UGA 5250), Institut de Chimie Moléculaire de Grenoble (ICMG, ER2607), Université Grenoble Alpes (UGA) 301 rue de la Chimie, BP 53, F-38041 Grenoble Cedex, FRANCE*

*e-mail: mark.casida@univ-grenoble-alpes.fr*

## Abstract

Singlet oxygen ( $^1\text{O}_2$ ) comes in two flavors — namely the dominant lower-energy  $a^1\Delta_g$  state and the higher-energy shorter-lived  $b^1\Sigma_g^+$  state — and plays a key role in many photochemical and photobiological reactions. For this reason, and because of the large size of the systems treated, many papers have appeared with density-functional theory (DFT) treatments of the reactions of  $^1\text{O}_2$  with different chemical species. The present work serves as a reminder that the common assumption that it is enough to fix the spin multiplicity as unity is not enough to insure a correct treatment of singlet oxygen. We review the correct group theoretical treatment of the three lowest energy electronic states of  $\text{O}_2$  which, in the case of  $^1\text{O}_2$  is often so badly explained in the relevant photochemical literature that the explanation borders on being incorrect and prevents, rather than encourages, a correct treatment of this interesting and important photochemical species. We then show how many electronic structure programs, such as a freely downloadable and personal-computer compatible LINUX version of DEMON2K, may be used, together with the multiplet sum method (MSM), to obtain a more accurate estimation of the potential energy curves (PECs) of the two  $^1\text{O}_2$  states. Applications of the MSM DFT method to  $^1\text{O}_2$  appear to be extremely rare as we were only able to find one correct application of the DFT MSM (or rather a very similar approach) to  $^1\text{O}_2$  in our literature search and then only using a single functional. Here we treat both the  $a^1\Delta_g$  and  $b^1\Sigma_g^+$  state with a wide variety of density-functional approximations (DFAs). Various strengths and weaknesses of different DFAs emerge through our application of the MSM method. In particular, the quality of the  $a^1\Delta_g$  excitation energy reflects how well functionals are able to describe the spin-flip energy in DFT while the quality of the  $b^1\Sigma_g^+$  excitation energy reflects how well functionals are able to describe the spin-pairing energy in DFT. Finally we note that improvements in DFT-based excited-state methods will be needed to describe the full PECs of  $^1\text{O}_2$  including both the equilibrium bond lengths and dissociation behavior.

# 1 Introduction

Modern chemistry is usually said to begin with the epoch of pneumatic chemistry when chemists realized that, rather than a single air, there are multiple airs (i.e., gases) which helped usher in the era of modern chemistry. Here “modern chemistry” may be roughly defined by Antoine-Laurent Lavoisier’s famous book [8] in which molecular oxygen, which makes up 20% of our atmosphere, plays a particularly important role. Those of us who teach first-year University chemistry are well aware that explaining the paramagnetism of  $O_2$  constitutes an early victory of molecular orbital (MO) theory. And yet, this diradical is not the highly-reactive species that experience with other radical species might lead us to believe. Indeed there is an important kinetic barrier [9] which prevents organic-based life forms such as we human beings from becoming interesting cases of spontaneous combustion. Yet  $O_2$  does react, with the right substances or given enough time or the right catalysts. This is why many metals are only found in the Earth’s crust as oxides. Moreover  $O_2$  is essential for respiration in animals which take in  $O_2$  and give off  $CO_2$  while plants produce  $O_2$  from  $CO_2$ . These examples indicate something about the richness of  $O_2$  chemistry and imply both that much must already be known about this well-studied molecule but also that there are good reasons why reactions of  $O_2$  will continue to be studied for some time to come. Molecular oxygen has three important low-lying states, namely the ground  $X^3\Sigma_g^-$  triplet state ( $^3O_2$ ) and the two low-lying electronic states of singlet oxygen ( $^1O_2$ ), the lower  $a^1\Delta_g$  state and the higher  $b^1\Sigma_g^-$  state. Several reviews have emphasized the importance of  $^1O_2$  for photochemistry and photobiology [1, 2, 3, 4, 5]. Unfortunately a basic understanding of the fundamental quantum chemistry of the processes involved in  $^1O_2$  reactions is hampered by the size of the systems interacting with  $^1O_2$  which are typically treated with a computationally-simplified (even if theoretically-sophisticated) method such as density-functional theory (DFT). Treating open-shell systems and excited-states with DFT is far from obvious for most users and so it is not surprising that almost all of the aforementioned applications are at best approximate (even conceptually incorrect). This is also true for DFT treatments of isolated  $^1O_2$ . It is the purpose of this paper to show how the Ziegler-Rauk-Baerends-Daul [6, 7] multiplet sum method (MSM) provides a simple first approximation to a correct treatment of  $^1O_2$ . We investigated a number of functionals and found which work best for this application. We also discuss limitations of the MSM and alternatives based upon DFT which may be able to overcome some of these limitations.

Much is already known about isolated  $^1O_2$ , making it a great molecule for validating DFT methodology but no longer a molecule which is interesting to study for its own sake. However there is still a great need to study how  $^1O_2$  reacts with other molecules and how  $^1O_2$  is created by excited photosensitizers reacting with  $^3O_2$ . Since we already have an interest in buckminsterfullerene ( $C_{60}$ ) [10, 11], let us mention, as an example, that  $C_{60}$  is of particular photochemical interest because it resists photodegradation and is not only a good electron acceptor but is also able to accept several electrons at a time. Also  $C_{60}$  is a photosensitizer [3] for creating  $^1O_2$  [12, 13]. Direct photoexcitation of  $^3O_2$  to form  $^1O_2$  is spectroscopically forbidden, but can be obtained by first photoexciting a different molecule (i.e., the photosensitizer) which can then transfer energy to  $^3O_2$  to make  $^1O_2$ . Yamakoshi *et al.* showed experimentally that  $C_{60}$  can act as just such a photosensitizer [14] and this photosensitization process was later investigated theoretically by Fueno *et al.* [15]. Once formed  $^1O_2$  is highly reactive and may react with many other molecules, including  $C_{60}$ .

The size of the  $C_{60} + O_2$  system combined with the accuracy and cost efficiency that we have come to expect from DFT means that DFT is one of the most common methods used to study this and similar problems. First, however, DFT must be properly validated for treating systems of this type which include both open-shell molecules and excited states. Very interestingly, although it is relatively easy to find DFT studies of the chemistry of  $^1O_2$  reacting with other molecules, it is

Table 1: Comparison of a few DFT  $a^1\Delta_g$  and  $b^1\Sigma_g^+$  excitation energies (Ha). Differences between vertical and adiabatic excitation energies (unspecified in this table) are small compared with the differences between the values obtained via different approaches.

Approach	$a^1\Delta_g$	$b^1\Sigma_g^+$	Reference
B3LYP/6-31G*	0.0166 <sup>a</sup> (0.0333 <sup>b</sup> )		Ref. [16]
B3LYP/6-31G*	0.0166 <sup>a</sup>		Ref. [15]
B3LYP/6-311G+(d,p)	0.0613 <sup>a</sup> (0.033 <sup>b</sup> )		Ref. [17]
HSEH1PBE/6-311G++(3df,2p)	0.0648 <sup>a</sup> (0.032 <sup>b</sup> )		Ref. [17]
B3PW91/6-311G++(3df,2p)	0.0632 <sup>a</sup> (0.032 <sup>b</sup> )		Ref. [17]
CAM-B3LYP/6-311G++(3df,2p)	0.0621 <sup>a</sup> (0.033 <sup>b</sup> )		Ref. [17]
M06/6-311G+(d,p)	0.0594 <sup>a</sup> (0.0503 <sup>b</sup> )		Ref. [17]
B97D3/TZVP S-T gap	0.0642		Ref. [18]
BLYP/DEF2-TZVPP $\pi_x[\uparrow\downarrow][\ ]\pi_y$	0.0568		PW <sup>c</sup>
BLYP/DEF2-TZVPP	0.0273	0.0863	PW <sup>c</sup>
M06/DEF2-TZVPP	0.0436	0.0674	PW <sup>c</sup>
MSDFT/M06-HF/cc-pVTZ	0.0430	0.0622	Ref. [19]
Best Estimate	0.0361	0.0658	Ref. [20]

<sup>a</sup> Broken-symmetry calculation.

<sup>b</sup> After spin projection using, for example, the method of Yamaguchi *et al.*

<sup>c</sup> Present work.

remarkably difficult to find benchmark studies validating different DFT methods for  $^1\text{O}_2$ . That is why the present work focuses uniquely on validating DFT for  $^1\text{O}_2$  before going on (in some other paper) to extending this methodology to  $^1\text{O}_2 + \text{C}_{60}$ . In order to see more clearly why this is needed, we have gathered values that we have found, as well as a few from the present work, into **Table 1**. The very large range of excitation energies seen in this table indicates that something is not quite right. Furthermore, besides the present work, we find only one other calculation of the  $b^1\Sigma_g^+$  excitation energy[19]. The usual approach used in the literature is to fix the spin multiplicity at one and carryout spin-unrestricted symmetry-broken DFT calculations. For example, this is the approach taken in the aforementioned article of Fueno *et al.* [15] who quote a a B3LYP excitation energy of 0.453 eV compared with a CASSCF value of 0.890 eV and an experimental value of 0.977 eV [1] for the  $^1\Delta_g$  state while we will show that the B3LYP MSM calculations give a  $^1\Delta_g$  excitation energy of 0.914 eV. In an earlier study [16], Garavelli *et al.* found that this value can be very much improved by spin-projection using the Yamaguchi method [21]. However our own experience with symmetry breaking in  $\text{H}_2$  (unpublished) is that one should not count on the Yamaguchi spin-projection method to improve results unless the spin-contamination is small as it can also make them worse. We are not alone in finding difficulties with the Yamaguchi spin-projection method [22, 23]. Nevertheless it is also the approach used in Ref. [17] (see the Supplementary Information for that article). The American National Institute of Standards and Technology (NIST) Computational Chemistry Comparison and Benchmark Data Base (CCCBDB) gives a value of the  $\text{O}_2$  singlet-triplet gap of 0.064204 Ha calculated at the B97D3/TZVP level [18]. This is clearly a very bad estimate of a true  $^3\text{O}_2 \rightarrow ^1\text{O}_2$  excitation energy but it does compare well with our calculations of the  $\pi_x[\uparrow][\ ]\pi_y \rightarrow \pi_x[\uparrow\downarrow][\ ]\pi_y$  energy (e.g., 0.05685 Ha with the BLYP functional.) In fact, besides our own, we know of only one study [19] which gives  $^1\text{O}_2$  energies of a similar quality to those of the MSM and

this is because the multistate DFT (MSDFT) method used there, though different from the MSM, has incorporated some aspects of the MSM. As the focus of that article was different from our own, only one functional was used. Here we show that different choices of density functionals can lead to significant differences in the quality of DFT MSM calculated  $^1\text{O}_2$  energies and potential energy curves (PECs), so that care in choosing the functional is important and compromises will likely have to be made. Fortunately studies such as the present one can help in making the choices and compromises.

We have yet another objective in writing this paper. Every research paper should be at least a little bit pedagogical in so far as the researcher needs to teach the reader what he or she has learned. In the present case, we wish to go a little further by showing an example of quality research based upon solid theoretical ideas but performed with inexpensive widely-available materials. Thus all of the calculations reported here could have been done (and should be reproducible) by anyone running LINUX using a freely downloadable version of the DEMON2K program [24].

This article is organized as follows: The electronic structure of  $^1\text{O}_2$  is reviewed in the next section, including the dissociation problem, and the MSM is presented. Section 3 presents key computational details and results are presented and discussed in Sec. 4. Section 5 presents conclusions and a discussion of perspectives for future work. Many more details are included in the *Supplementary Information* in order to make our presentation particularly complete.

## 2 Theory

We would like to use DFT to calculate the three lowest potential energy curves (PECs) for  $\text{O}_2$ . Accurate representations are shown in **Fig. 1**. (See also Refs. [26, 27, 28].) Specifically, these are the  $^3\Sigma_g^-$  ground state, the lowest  $^1\Delta_g$  singlet state, and a higher  $^1\Sigma_g^+$  excited state. They arise from the different ways that two electrons may be placed into the two  $\pi^*$  orbitals of the molecule. In this section, we will first review the minimal configurations needed to describe these three states in the context of wave function theory, then discuss the problem of correctly dissociating  $\text{O}_2$ , and finally we will describe how the  $^3\Sigma_g^-$ ,  $^1\Delta_g$ , and  $^1\Sigma_g^+$  may be calculated using DFT near the equilibrium geometry.

### 2.1 Wave function theory

**Figure 2** should be familiar. It summarizes the molecular-orbital (MO) picture of  $\text{O}_2$  that most of us learn in our first-year University chemistry course. It is a rather famous observation that, though the Lewis dot structure seems to indicate that all electrons are paired, MO theory shows that the ground state of  $\text{O}_2$  is, in fact, a triplet ( $^3\text{O}_2$ ). Nevertheless, the calculation of the bond order index still shows a double bond.

Low-lying excited states arise from the six symmetry-adapted linear combinations (SALCs) of the six different ways to put two electrons in the two  $\pi^*$  orbitals:

$$\begin{array}{ll}
 \pi_x^*[\uparrow \ ] & [\uparrow \ ]\pi_y^* \\
 \pi_x^*[\uparrow\downarrow] & [ \ ]\pi_y^* \\
 \pi_x^*[\ \uparrow] & [ \downarrow]\pi_y^* \\
 \pi_x^*[\ \downarrow] & [\uparrow \ ]\pi_y^* \\
 \pi_x^*[\ \ ] & [\uparrow\downarrow]\pi_y^* \\
 \pi_x^*[\ \downarrow] & [ \downarrow]\pi_y^*
 \end{array}
 \tag{1}$$

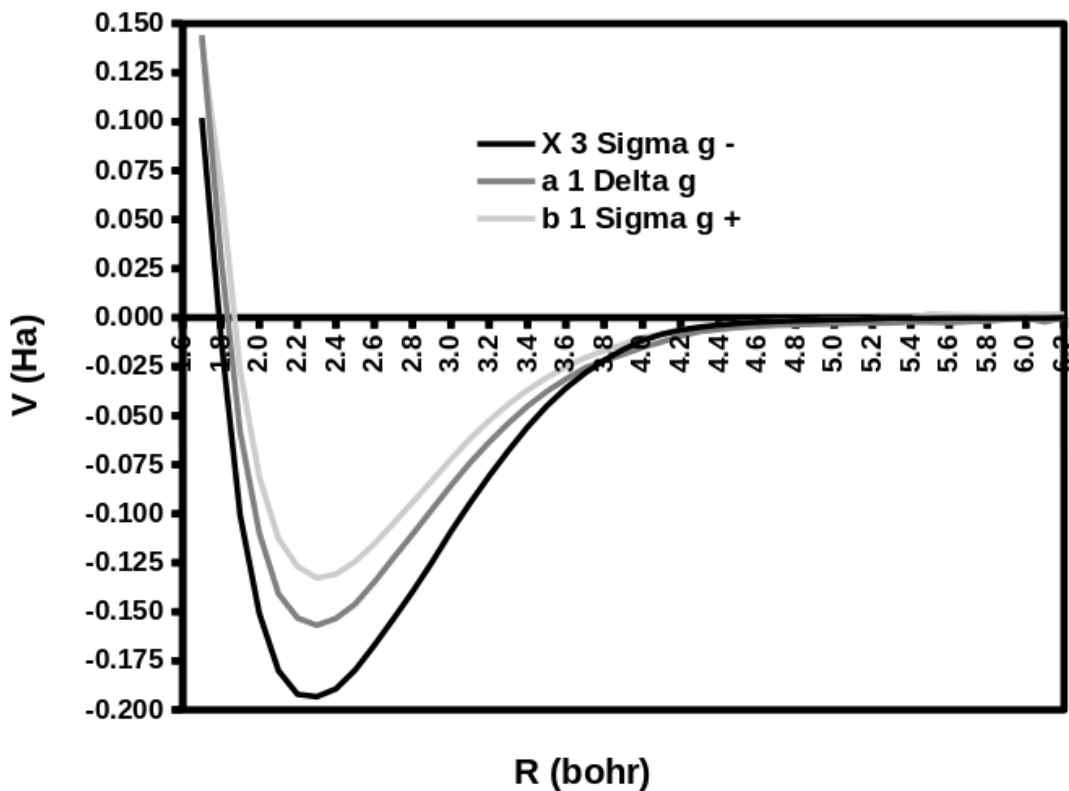


Figure 1: Potential energy curves for the three lowest electronic states of  $O_2$ , namely  $X^3\Sigma_g^-$ ,  $a^1\Delta_g$ , and  $b^1\Sigma_g^+$ , from Fig. 1 of Ref. [20] digitized with WEBPLOTDIGITIZER [25] and redrawn. The zero of energy is the twice the energy of the  $O(^3P)$  atom.

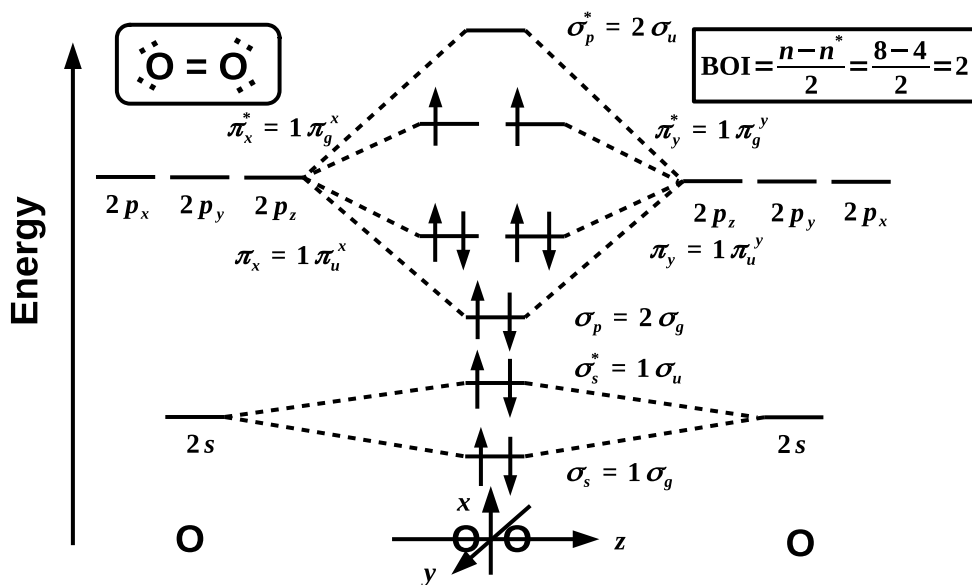


Figure 2: First-year University description of the electronic structure of  $O_2$ : atomic orbital/molecular orbital correlation diagram, Lewis dot structure (upper left inset), and calculation of the bond order index (BOI, upper right inset.)

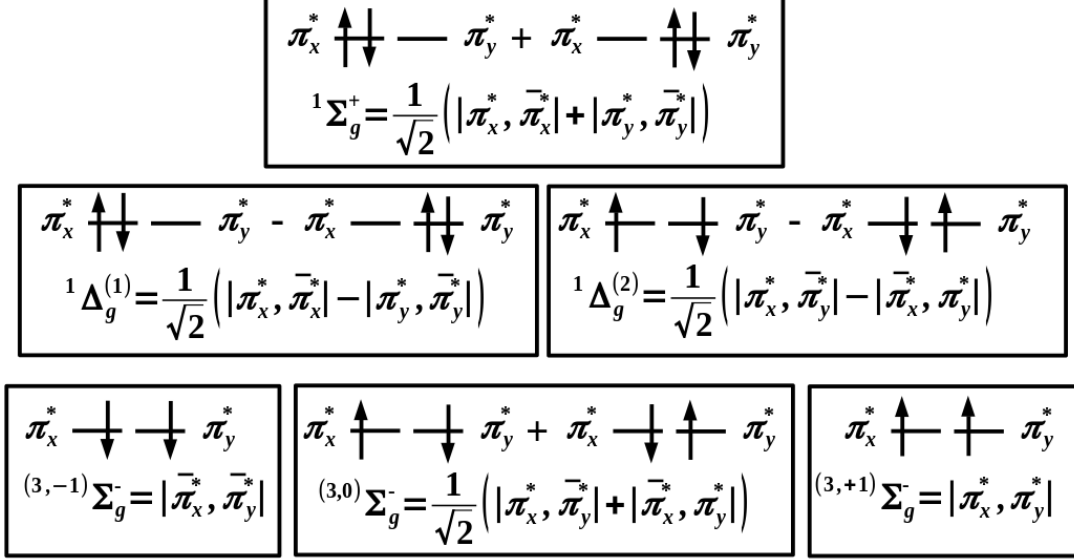


Figure 3: Practical representation of the lowest three electronic states of O<sub>2</sub> using real-valued MOs.

Making the SALCs requires the recognition that homonuclear diatomics like O<sub>2</sub> belong to the  $D_{\infty h}$  point group whose character table is given in the *Supplementary Information*. At the orbital level, the use of group theory does not change very much, except that the MOs are now labeled as  $g$  (*gerade*) or  $u$  (*ungerade*) according to their inversion symmetry. Figure 2 shows both the usual bonding and antibonding and the group theoretic nomenclature for the MOs. We will be using both types of nomenclature.

The many-electron state symmetry is determined by the orbitals outside the closed-shell — that is, by linear combinations of determinants of with different occupations of the  $\pi_x^* = \pi_g^x$  and  $\pi_y^* = \pi_g^y$ . (See the *Supplementary Information* for a group theoretic construction of the SALCs.) The result is summarized in **Fig. 3** and is the representation that we will use in the present work.

However this is not the representation which is used in most of the literature. Instead, the conventional analysis for O<sub>2</sub> (see, e.g., Ref. [1]) uses the complex-valued orbitals,

$$\begin{aligned} \pi_-^* &= \frac{1}{\sqrt{2}} (\pi_x^* - i\pi_y^*) \\ \pi_+^* &= \frac{1}{\sqrt{2}} (\pi_x^* + i\pi_y^*) . \end{aligned} \quad (2)$$

This leads to the conventional representation of the lowest three electronic states shown in **Fig. 4**.

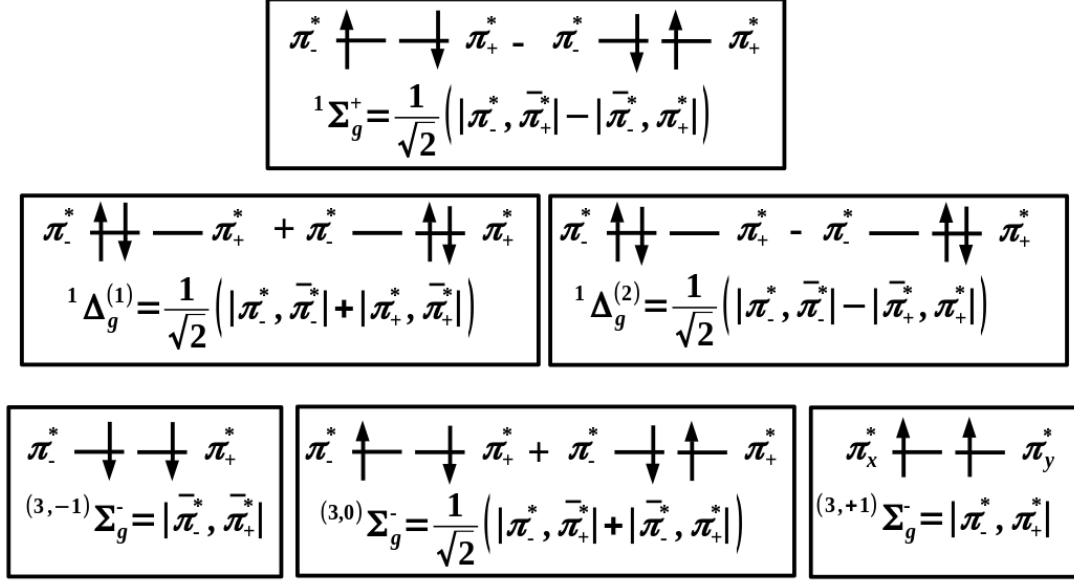


Figure 4: Conventional representation of the lowest three electronic states of O<sub>2</sub> using complex-valued MOs.

Note that the MOs in Figs. 4 and 3 differ by phase factors:

$$\begin{aligned}
|\pi_-^*, \pi_+^*| &= i|\pi_x^*, \pi_y^*| \\
\frac{1}{\sqrt{2}} (|\pi_-^*, \bar{\pi}_+^*| + |\bar{\pi}_-^*, \pi_+^*|) &= \frac{i}{\sqrt{2}} (|\pi_x^*, \bar{\pi}_y^*| + |\bar{\pi}_x^*, \pi_y^*|) \\
|\bar{\pi}_-^*, \bar{\pi}_+^*| &= i|\bar{\pi}_x^*, \bar{\pi}_y^*| \\
\frac{1}{\sqrt{2}} (|\pi_-^*, \bar{\pi}_-^*| + |\pi_+^*, \bar{\pi}_-^*|) &= \frac{1}{\sqrt{2}} (|\pi_x^*, \bar{\pi}_x^*| - |\pi_y^*, \bar{\pi}_y^*|) \\
\frac{1}{\sqrt{2}} (|\pi_-^*, \bar{\pi}_-^*| - |\pi_+^*, \bar{\pi}_-^*|) &= \frac{i}{\sqrt{2}} (|\bar{\pi}_x^*, \pi_y^*| - |\pi_x^*, \bar{\pi}_y^*|) \\
\frac{1}{\sqrt{2}} (|\pi_-^*, \bar{\pi}_+^*| - |\bar{\pi}_-^*, \pi_+^*|) &= \frac{1}{\sqrt{2}} (|\pi_x^*, \bar{\pi}_x^*| + |\pi_y^*, \bar{\pi}_y^*|) , \tag{3}
\end{aligned}$$

but are otherwise equivalent. Unfortunately, though this convention is widely used [29, 3, 5, 30], it is now also only rarely explained and the  $\pi$  orbitals are hardly ever properly labeled (see however Ref. [31, 4]). We will use the real  $\pi_x^*$  and  $\pi_y^*$  MOs in the present work, rather than the complex valued  $\pi_-^*$  and  $\pi_+^*$  MOs, as most quantum chemistry programs use real MOs.

## 2.2 Dissociation limit

As we will be calculating PECs, we should also look at the dissociation limit. A prelude to this is to work out the possible atomic term symbols. There are many ways to do this, including, for example, Hyde's very teachable double ladder method [33]. The result may be expressed in terms of Russell-Saunders coupling of the spin and orbital magnetic moments. The term symbol takes the form  ${}^{2S+1}L_J$  where

$$J = L + S, L + S - 1, \dots, |L - S| , \tag{4}$$

Table 2: Term symbols and relative energies of  $2p^4$  multiplets of the oxygen atom from the Atomic Spectra Database of the American National Institute of Standards and Technology [32].

Term	$J$	Energy	
		$\text{cm}^{-1}$	eV
$^1S$	0	33 792.483	4.1897359
$^1D$	2	15 867.862	1.9673651
$^3P$	0	226.977	0.0281416
	1	158.265	0.0196224
	2	0.000	0.0000000

is a new label used to distinguish the different levels with the same  $L$  and  $S$ . Whichever way is used to derive the atomic term symbols, the result is that shown in **Table 2**. Hund's rules tell us that the ground state of the oxygen atom should be  $^3P$ . Although Hund's rules do not in general apply to excited states, they do give the proper ordering of atomic states in the present case even for the excited states listed in the table.

Let us now consider the problem of dissociating  $\text{O}_2$ . According to Ref. [20] (and other sources) the  $^3\Sigma_g^-$ ,  $^1\Delta_g$ , and  $^1\Sigma_g^+$  states all dissociate into two  $^3P$  atoms. Let us try to figure out how this works for the  $^3\Sigma_g^-$  state. This is basically an exercise in how molecular orbital theory is connected with valence bond theory which can be represented by Lewis representations. As we will be putting linear combinations of Slater determinants inside Slater determinants, we should take a moment to clarify what is meant by a determinant within a determinant. As the determinant of a matrix and the determinant of the transpose of a determinant are the same, we could define a Slater determinant either by,

$$|\psi_1, \psi_2, \dots, \psi_N| = \frac{1}{\sqrt{N!}} \sum_{\sigma \in \mathcal{S}_N} (-1)^\sigma \psi_{\sigma(1)}(1) \psi_{\sigma(2)}(2) \cdots \psi_{\sigma(N)}(N), \quad (5)$$

or by,

$$|\psi_1, \psi_2, \dots, \psi_N| = \frac{1}{\sqrt{N!}} \sum_{\sigma \in \mathcal{S}_N} (-1)^\sigma \psi_1(\sigma(1)) \psi_2(\sigma(2)) \cdots \psi_N(\sigma(N)), \quad (6)$$

where  $\mathcal{S}_N$  is the symmetric group for (i.e., the group of permutation of) the numbers  $1, 2, \dots, N$  and  $(-1)^\sigma$  is the sign of the permutation. Only the second definition of the Slater determinant is suitable for a general function. Thus we may write that,

$$|f(1, 2, \dots, N)| = \frac{1}{\sqrt{N!}} \sum_{\sigma \in \mathcal{S}_N} (-1)^\sigma f(\sigma(1), \sigma(2), \dots, \sigma(N)). \quad (7)$$

It is then a relatively simple exercise in group theory to show that,

$$||\psi_1, \psi_2, \dots, \psi_P|, \psi_{P+1}, \psi_N| = \sqrt{P!} |\psi_1, \psi_2, \dots, \psi_N|. \quad (8)$$

We also need that determinants are linear so that, for example,

$$|\psi_1, \psi_2, \dots, C_a \psi_a + C_b \psi_b, \dots, \psi_N| = C_a |\psi_1, \psi_2, \dots, \psi_a, \dots, \psi_N| + C_b |\psi_1, \psi_2, \dots, \psi_b, \dots, \psi_N|. \quad (9)$$

This latter allows us to replace  $p_{\pm 1}$  with  $p_x$  and  $p_y$  using the relations,

$$\begin{aligned} p_x &= \frac{1}{\sqrt{2}}(p_{+1} + p_{-1}) \\ p_y &= \frac{1}{i\sqrt{2}}(p_{+1} - p_{-1}) . \end{aligned} \quad (10)$$

In particular,

$$|p_x, p_y| = +i|p_{+1}, p_{-1}| \quad (11)$$

differ only by a phase factor. Recall also that  $p_0 = p_z$ .

We may now make a connection with chemical bonding and in particular with chemical bond breaking. Orbitals  $\chi_A$  and  $\chi_B$  on two different centers  $A$  and  $B$  may form bonding and antibonding combinations,

$$\psi_{\pm} = \frac{1}{\sqrt{2}}(\chi_A \pm \chi_B) . \quad (12)$$

Here we have assumed that we are only interested in the dissociation limit when the two centers are so far apart that any overlap between  $\chi_A$  and  $\chi_B$  is large enough to be able to define what is meant between bonding and antibonding but small enough to be neglected in the normalization. Note also that which of the plus and minus combinations is bonding and which is antibonding depends upon the precise nature of the orbitals  $\chi_A$  and  $\chi_B$ . Filling both the bonding and antibonding combinations is equivalent to bond breaking because,

$$|\psi_+, \psi_-| = -|\chi_A, \chi_B| . \quad (13)$$

This is why these terms cancel when calculating the bond order index (BOI =  $(n - n^*)/2$ , where  $n$  is the number of electrons in bonding orbitals and  $n^*$  is the number of electrons in antibonding orbitals.) Referring back to Fig. 2, we see that we already have in the dissociation limit that, dropping unimportant phase factors,

$$|\sigma, \bar{\sigma}, \sigma^*, \bar{\sigma}^*, \sigma_p, \bar{\sigma}_p, \pi_x, \bar{\pi}_x, \pi_y, \bar{\pi}_y, \pi_x^*, \pi_y^*| \rightarrow |s_A, \bar{s}_A, s_B, \bar{s}_B, \sigma_p, \bar{\sigma}_p, p_x^A, \bar{p}_x^B, p_y^A, \bar{p}_y^B, \pi_x, \bar{\pi}_y| . \quad (14)$$

Dissociating the  $\sigma_p$  bond is a bit more complicated. As the diatomic molecule traditionally lies along the  $z$ -axis, we have that

$$\begin{aligned} \sigma_p &= \frac{1}{\sqrt{2}}(p_z^A - p_z^B) \\ \sigma_p^* &= \frac{1}{\sqrt{2}}(p_z^A + p_z^B) . \end{aligned} \quad (15)$$

This leads to

$$\frac{1}{\sqrt{2}}(-|\sigma_p, \bar{\sigma}_p| + |\sigma_p^*, \bar{\sigma}_p^*|) = \frac{1}{\sqrt{2}}(|p_z^A, \bar{p}_z^B| - |\bar{p}_z^A, p_z^B|) , \quad (16)$$

which is proper dissociation. Hence (dropping phase factors)

$$\begin{aligned} &\frac{1}{\sqrt{2}}|\sigma, \bar{\sigma}, \sigma^*, \bar{\sigma}^*, \frac{1}{\sqrt{2}}(-|\sigma_p, \bar{\sigma}_p| + |\sigma_p^*, \bar{\sigma}_p^*|), \pi_x, \bar{\pi}_x, \pi_y, \bar{\pi}_y, \pi_x^*, \pi_y^*| \\ \rightarrow &\frac{1}{\sqrt{2}}|s_A, \bar{s}_A, s_B, \bar{s}_B, p_z^A, \bar{p}_z^B, p_x^A, p_x^B, p_y^A, p_y^B, \pi_x, \bar{\pi}_y| \\ - &\frac{1}{\sqrt{2}}|s_A, \bar{s}_A, s_B, \bar{s}_B, \bar{p}_z^A, p_z^B, p_x^A, p_x^B, p_y^A, p_y^B, \pi_x, \bar{\pi}_y| . \end{aligned} \quad (17)$$

Getting proper atomic dissociation into  ${}^3P$  components requires us to use that,

$$\begin{aligned}
\bar{\pi}_x &= \bar{p}_x^A + \bar{p}_x^B \\
\bar{\pi}_x^* &= \bar{p}_x^A - \bar{p}_x^B \\
\bar{\pi}_y &= \bar{p}_y^A + \bar{p}_y^B \\
\bar{\pi}_y^* &= \bar{p}_y^A - \bar{p}_y^B .
\end{aligned} \tag{18}$$

Then

$$\frac{1}{\sqrt{2}} (|\bar{\pi}_x, \bar{\pi}_y| - |\bar{\pi}_x^*, \bar{\pi}_y^*|) = \frac{1}{\sqrt{2}} (|\bar{p}_x^A, \bar{p}_y^B| + |\bar{p}_y^A, \bar{p}_x^B|) . \tag{19}$$

Hence

$$\begin{aligned}
& \frac{1}{2} |\sigma, \bar{\sigma}, \sigma^*, \bar{\sigma}^*|, \frac{1}{\sqrt{2}} (|\sigma_p, \bar{\sigma}_p| + |\sigma_p^*, \bar{\sigma}_p^*|), \pi_x, \bar{\pi}_x, \pi_y, \bar{\pi}_y, \frac{1}{\sqrt{2}} (|\bar{\pi}_x, \bar{\pi}_y| - |\bar{\pi}_x^*, \bar{\pi}_y^*|) | \\
\rightarrow & \frac{1}{2} |s_A, \bar{s}_A, s_B, \bar{s}_B, p_z^A, \bar{p}_z^B, p_x^A, p_x^B, p_y^A, p_y^B, \bar{p}_x^A, \bar{p}_y^B| \\
& + \frac{1}{2} |s_A, \bar{s}_A, s_B, \bar{s}_B, p_z^A, \bar{p}_z^B, p_x^A, p_x^B, p_y^A, p_y^B, \bar{p}_y^A, \bar{p}_x^B| \\
& - \frac{1}{2} |s_A, \bar{s}_A, s_B, \bar{s}_B, \bar{p}_z^A, p_z^B, p_x^A, p_x^B, p_y^A, p_y^B, \bar{p}_x^A, \bar{p}_y^B| \\
& - \frac{1}{2} |s_A, \bar{s}_A, s_B, \bar{s}_B, \bar{p}_z^A, p_z^B, p_x^A, p_x^B, p_y^A, p_y^B, \bar{p}_y^A, \bar{p}_x^B| ,
\end{aligned} \tag{20}$$

which is a sum of four terms each corresponding to two  ${}^3P$  oxygen atoms. (Compare with Fig. 43 of Ref. [34].)

The only wave function in ordinary DFT is that of the reference system of non-interacting electrons which is single-determinantal for a non-degenerate system. This is why DFT is assumed to work best for systems which can be described to a first approximation by a single-determinantal wave function. This is clearly not the case for the dissociation limit of the  ${}^3O_2$  ground state. However, as is commonly illustrated for  $H_2$ , we may often obtain a reasonable approximation to the ground state PEC by symmetry breaking in spin-unrestricted DFT calculations. Hence, for  ${}^3O_2$  we can imagine calculating the PEC by symmetry breaking and using a  $|s_A, \bar{s}_A, s_B, \bar{s}_B, p_z^A, \bar{p}_z^B, p_x^A, p_x^B, p_y^A, p_y^B, \bar{p}_y^A, \bar{p}_x^B|$  (i.e.,  $|s_A, \bar{s}_A, p_x^A, p_y^A, \bar{p}_y^A, p_z^A|$  and  $|s_B, \bar{s}_B, p_x^B, \bar{p}_x^B, p_y^B, \bar{p}_z^B|$ ).

We should emphasize the difficulties with applying symmetry breaking in this case. As molecules become more complex, there may be more than one way to lower the energy by symmetry breaking. Finding the different ways to break symmetry and choosing the best one is, as far as we know, an unsolved problem. The problem of multiple ways to break symmetry is likely to be relevant for  ${}^3O_2$  as it is not enough to break the  $\sigma_p$  or  $\pi_x$  or  $\pi_y$  symmetries but we also have to break them all simultaneously in the right way, which is not at all an obvious thing to do.

The situation is more severe when trying to use DFT to treat the dissociation limit of excited states. This is because the MOs no longer belong to well-defined irreducible representations of the point group, making it difficult to assign the symmetries of any excited states made from these MOs.

## 2.3 Singlet States from the Multiplet Sum Method

Although DFT seems to only work for states which may be described by a single-determinant reference, we may obtain the energies of other states using the Ziegler-Rauk-Baerends (Daul) multiplet sum method (MSM) [6, 7]. This works for single-point (i.e., at a single geometry) calculations but

we are only aware of one implementation of analytic gradients which would allow geometry optimizations with this method Friedrichs and Frank used such a method in the CPMD program to do excited-state dynamics [36].

To see how to apply the MSM, we will consider the three  ${}^3\Sigma_g^-$  wavefunctions,

$$\begin{aligned} ({}^{3,1})\Sigma_g^- &= |\pi_x^*, \pi_y^*| \\ ({}^{3,0})\Sigma_g^- &= \frac{1}{\sqrt{2}} (|\pi_x^*, \bar{\pi}_y^*| + |\bar{\pi}_x^*, \pi_y^*|) \\ ({}^{3,-1})\Sigma_g^- &= |\bar{\pi}_x^*, \bar{\pi}_y^*|, \end{aligned} \quad (21)$$

and the two  ${}^1\Delta_g$  wavefunctions,

$$\begin{aligned} {}^1\Delta_g^{(1)} &= \frac{1}{\sqrt{2}} (|\pi_x^*, \bar{\pi}_x^*| - |\bar{\pi}_y^*, \pi_y^*|) \\ {}^1\Delta_g^{(2)} &= \frac{1}{\sqrt{2}} (|\pi_x^*, \bar{\pi}_y^*| - |\bar{\pi}_x^*, \pi_y^*|). \end{aligned} \quad (22)$$

Then

$$\begin{aligned} E[{}^3\Sigma_g^-] &= E[({}^{3,0})\Sigma_g^-] = E[|\pi_x^*, \bar{\pi}_y^*|] + \langle |\pi_x^*, \bar{\pi}_y^*| | \hat{H} | |\bar{\pi}_x^*, \pi_y^*| \rangle \\ E[{}^1\Delta_g] &= E[{}^1\Delta_g^{(2)}] = E[|\pi_x^*, \bar{\pi}_y^*|] - \langle |\pi_x^*, \bar{\pi}_y^*| | \hat{H} | |\bar{\pi}_x^*, \pi_y^*| \rangle. \end{aligned} \quad (23)$$

Hence,

$$E[{}^3\Sigma_g^-] + E[{}^1\Delta_g] = 2E[|\pi_x^*, \bar{\pi}_y^*|], \quad (24)$$

and,

$$\begin{aligned} E[{}^1\Delta_g] &= 2E[|\pi_x^*, \bar{\pi}_y^*|] - E[{}^3\Sigma_g^-] \\ &= 2E[|\pi_x^*, \bar{\pi}_y^*|] - E[({}^{3,0})\Sigma_g^-] \\ &= 2E[|\pi_x^*, \bar{\pi}_y^*|] - E[|\pi_x^*, \pi_y^*|]. \end{aligned} \quad (25)$$

Thus the  ${}^1\Delta_g$  energy has been expressed purely in terms of the energies of two single-determinantal states—namely the fictitious mixed-symmetry  $|\pi_x^*, \bar{\pi}_y^*|$  state and the triplet state  $|\pi_x^*, \pi_y^*|$ . In principle, these should all be calculated using the same MOs derived from some reference calculation (see below.)

In principle the extension of the MSM to the

$${}^1\Sigma_g^+ = \frac{1}{\sqrt{2}} (|\pi_x^*, \bar{\pi}_x^*| + |\pi_y^*, \bar{\pi}_y^*|) \quad (26)$$

is just as straightforward as

$$\begin{aligned} E[{}^1\Sigma_g^+] &= E[|\pi_x^*, \bar{\pi}_x^*|] + \langle |\pi_x^*, \bar{\pi}_x^*| | \hat{H} | |\pi_y^*, \bar{\pi}_y^*| \rangle \\ E[{}^1\Delta_g] &= E[{}^1\Delta_g^{(1)}] = E[|\pi_x^*, \bar{\pi}_x^*|] - \langle |\pi_x^*, \bar{\pi}_x^*| | \hat{H} | |\pi_y^*, \bar{\pi}_y^*| \rangle. \end{aligned} \quad (27)$$

So,

$$E[{}^1\Sigma_g^+] + E[{}^1\Delta_g] = 2E[|\pi_x^*, \bar{\pi}_x^*|], \quad (28)$$

and

$$E[{}^1\Sigma_g^+] = 2E[|\pi_x^*, \bar{\pi}_x^*|] - E[{}^1\Delta_g]. \quad (29)$$

For the reader’s convenience, we will repeat the key formulae again but this time in a somewhat different and more physically more picturesque manner:

$$\begin{aligned}
E[X^3\Sigma_g^-] &= E(\pi_x^*[\uparrow, \downarrow], [\uparrow, \downarrow]\pi_y^*) \\
E[a^1\Delta_g] &= E(\pi_x^*[\uparrow, \downarrow], [\uparrow, \downarrow]\pi_y^*) + 2F \\
E[b^1\Sigma_g^+] &= E(\pi_x^*[\uparrow, \downarrow], [\uparrow, \downarrow]\pi_y^*) + 2P,
\end{aligned}
\tag{30}$$

where the spin-flip energy,

$$F = E(\pi_x^*[\uparrow, \downarrow], [\uparrow, \downarrow]\pi_y^*) - E(\pi_x^*[\uparrow, \uparrow], [\uparrow, \downarrow]\pi_y^*) \tag{31}$$

and the spin-pairing energy

$$P = E(\pi_x^*[\uparrow, \downarrow], [\uparrow, \downarrow]\pi_y^*) - E(\pi_x^*[\uparrow, \uparrow], [\uparrow, \downarrow]\pi_y^*). \tag{32}$$

This way of writing the equations tells us that the  $X^3\Sigma_g^- \rightarrow a^1\Delta_g$  excitation is going to be sensitive to how well a given density-functional approximation (DFA) can describe spin-flip energies and that the  $X^3\Sigma_g^- \rightarrow b^1\Sigma_g^+$  excitation is going to be sensitive to how well a given DFA can describe spin-pairing energies.

## 2.4 Reference State Problem

As noted above, ideally the MSM should make use of a single set of MOs coming from some reference calculation. The choice of reference calculation may be governed by several factors, including ease of convergence. However, it should be emphasized that the reason for using a reference state is not just that some calculations converge more easily than others. The reference calculation also guarantees that the different determinants which are created are properly orthogonal to each other so as to avoid variational collapse. The same problem is addressed in complete active state self-consistent field (CAS-SCF) calculations by using state averaging. Of course, the price that has to be paid is that orbital relaxation is neglected, which is not always a good thing.

Let us now turn our attention specifically to  $^1O_2$ . The result of specifying a spin multiplicity of one and running a calculation is that most programs will try to pair up electrons by putting two electrons in a single  $\pi^*$  orbital. Such a doubly-occupied  $\pi^*$  orbital will no longer be energetically degenerate with the other (empty)  $\pi^*$  orbital. In fact, the occupied  $\pi^*$  orbital will have a higher energy than the unoccupied  $\pi^*$  orbital because of self-interaction errors. Formal DFT predicts that this can happen in open-shell systems even for the exact functional when noninteracting  $v$ -representability (NVR) fails. We call this an effective failure of NVR when it occurs for an approximate functional [37]. In either case, the result is that most programs will try to satisfy the *Aufbau* principle at each iteration by transferring electrons from the higher-energy occupied  $\pi^*$  orbital to the lower-energy unoccupied  $\pi^*$  orbital. As this then raises the energy of the newly occupied orbital and lowers the energy of the newly unoccupied orbital, we have an unstable situation and the calculations will typically no longer converge.

This problem may be solved by creating a reference state with each  $\pi^*$  orbital having half a spin-up and half spin-down electron. Most programs have an option which allows the user to create this fractionally-occupied state easily. Here we used the DEMON2K program [38, 24]. In this program, it suffices to use the keyword combination `SMEAR 0.1 UNIFORM` where the number 0.1 is an adjustable number in eV which controls how close orbitals are in energy before they are uniformly occupied. *A priori* this type of fractionally-occupied state corresponds to some sort of ensemble electronic

state, where the ensemble average has been carried out over several multiplet states. However deeper thought indicates that this conclusion is far from obvious. Another possibility (not tried) would be to use a carefully-selected restricted open-shell Kohn-Sham (ROKS) calculation as a reference state. Once such a reference state is created, electrons may be displaced to create different occupation states without additional iterations. In DEMON2K, this is done with the keywords SCFTYPE UKS MAX=0 and MOMODIFY.

### 3 Computational Details

This is a very short section as much of the computational method has either been described in the Theory Section (Sec. 2), in the *Supplementary Material*, or will be described in the Results Section (Sec. 4). We used a Gaussian-type orbital (GTO) based quantum chemistry code which makes use of both GTO-type basis functions for expanding the molecular orbitals but also uses GTO-type basis functions to expand the density (for local DFAs) and the density matrix (for hybrid DFAs) in order to eliminate four-center electron repulsion integrals. In particular, we used version 5.0 of DEMON2K which is freely downloadable from the web site and runs under LINUX [38]. The code is described in more detail in Refs. [24, 39]. Our calculations used the DEF2-TZVPP orbital basis set and the GEN-A3\* auxiliary basis set. Nearly all the functionals available in this particular version of DEMON2K were used. (No Hartree calculations were performed.) Literature citations for the specific functionals may be found in the Tables in the *Supplementary Material*. For other parameters, we simply made extensive use of default options. Occasionally we made use of convergence options other than the default when this seemed useful. Atomic  $O(^3P)$  energies were calculated at the same level as for diatomic  $O_2$ . No correction was made for basis set superposition error. Nearly all calculations were done without symmetry breaking and a sample input file has been included in the *Supplementary Material* for those who wish to reproduce our calculations. Calculations with symmetry breaking used a somewhat different procedure which is described in Sec. 4 though our purpose in describing symmetry broken calculations is primarily to caution against them.

### 4 Results

We wish to investigate the strengths and limitations of different density-functional approximations (DFAs) for use with the multiplet sum method (MSM) for treating the first three states ( $X^1\Sigma_g^-$ ,  $a^1\Delta_g$ , and  $b^1\Sigma_g^+$ ) of  $O_2$ . These calculations could be carried out with just about any DFT program, but we wish to be simultaneously both pedagogic and to show that quality research can be done even with limited computer resources, so we have chosen to use a freely downloadable and personal-computer compatible LINUX version of DEMON2K. Also for pedagogical clarity, after briefly reviewing our source of *best estimate* comparison data, we will spend a bit of time showing what happens when the method is applied in combination with symmetry breaking. This is important because many people try to deal with problems in DFT through symmetry breaking and we wish to discuss why this fails through a concrete example. We will then go on to compare MSM calculations for  $O_2(X^1\Sigma_g^-)$ ,  $O_2(a^1\Delta_g)$ , and  $O_2(b^1\Sigma_g^+)$  without symmetry breaking using various functionals. Finally we will choose one of the better functionals and compare our MSM PECs with our reference PECs. Unless otherwise specified, results will be given in Hartree atomic units ( $\hbar = m_e = e$ ). This is simply convenient when interconverting large amounts of data. Results are summarized graphically here, but tables of calculated values may be found in the *Supplementary Information* where references may also be found for the functionals used in the present paper.

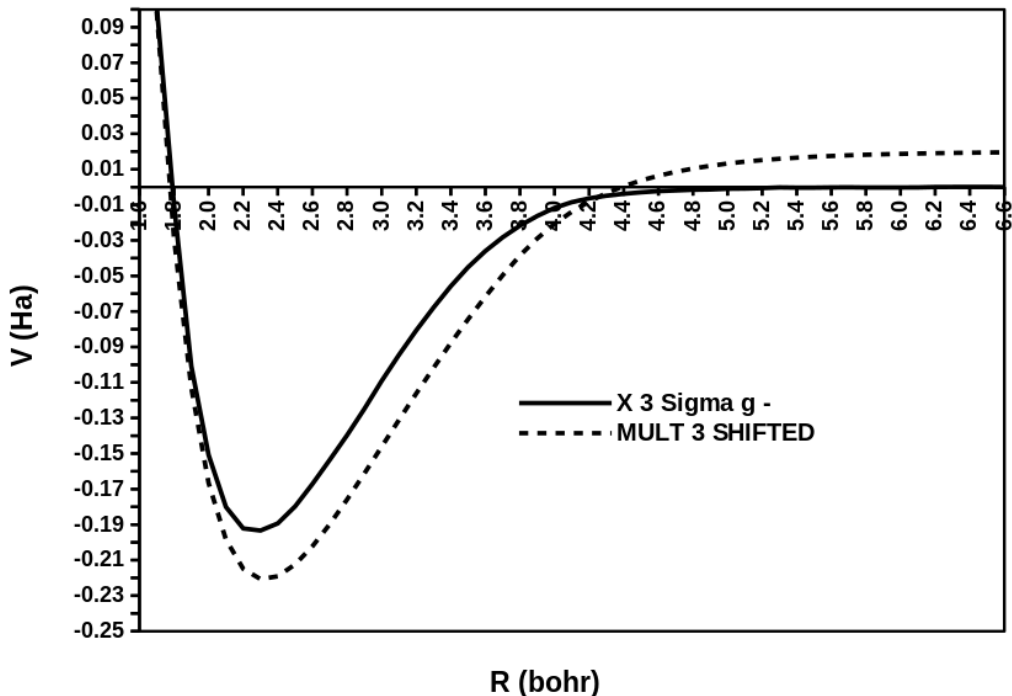


Figure 5:  $\text{O}_2(X^3\Sigma_g^-)$  PECs calculated using the symmetry breaking procedure described in the text: best estimate, solid line; broken symmetry BLYP, dashed line. The zero of energy is that of twice the energy of a single  $\text{O}(^3P)$  atom without any basis set superposition error (BSSE) correction.

## 4.1 Choice of Best Estimate Comparison Data

Because of the great importance of  $\text{O}_2$ , there are many reference studies — in fact, too many to discuss specifically here. Some particularly notable reviews are Refs. [26, 27, 28]. We found it particularly convenient to digitize data from Fig. 1 of Ref. [20]. These data are given in the *Supplementary Information* and regraphed in Fig. 1. Another useful source of comparison data is the American National Institute of Standards and Technologies (NIST) Atomic Spectra Database [32] to which we will also sometimes refer.

## 4.2 With Symmetry Breaking

This works best in the case of the  $\text{O}_2(X^3\Sigma_g^-)$  ground state and becomes almost nonsensical for the  $\text{O}_2(a^1\Delta)$  and  $\text{O}_2(b^1\Sigma_g^+)$  excited states.

Let us begin with the ground  $\text{O}_2(X^3\Sigma_g^-)$  state. As discussed in Sec. 2.2, breaking symmetry to obtain the correct dissociation limit of  $\text{O}_2$  into two ground-state  $\text{O}(^3P)$  atoms is anything but obvious. As it happened, it was possible to first generate a restart file from a calculation for a single  $\text{O}(^3P)$  atom and then use this as an initial guess for an SCF calculation at large internuclear distance. We then gradually reduced the  $\text{O}_2$  bond length using the the restart file from the previous (slightly longer) bond length as the initial guess for our SCF calculation. The results are shown in **Fig. 5**. The general shape of the BLYP PEC is correct but it dissociates to a higher energy than twice the energy of two oxygen atoms, suggesting that further symmetry breaking might be possible. (Or perhaps this is simply the best that can be done without resorting to a multideterminantal approach?) It is

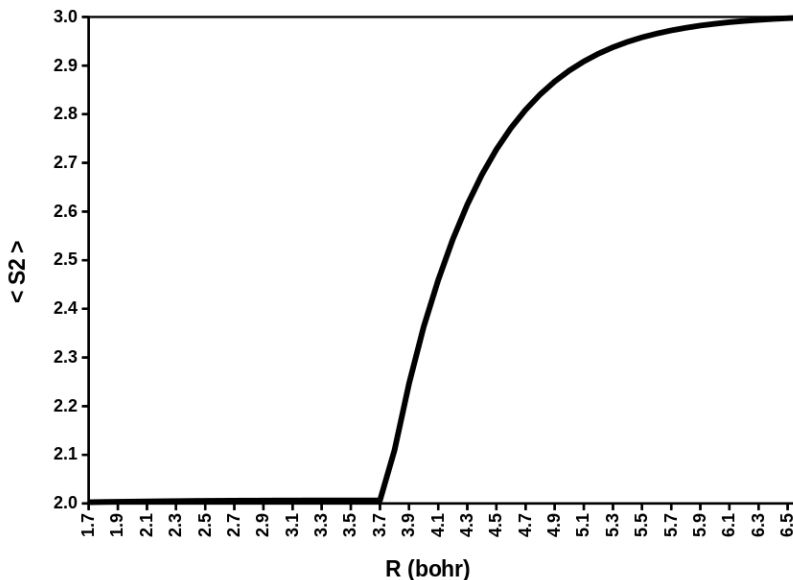


Figure 6:  $O_2(X^3\Sigma_g^-)$   $\langle \hat{S}^2 \rangle$  for the symmetry broken calculation.

also clear that BLYP overbinds the molecule.

Not all of the curve shown in Fig. 5 is symmetry broken. Symmetry breaking only occurs when there is a symmetry-broken [different-orbitals-for-different-spin (DODS)] solution which is lower in energy than the symmetry-unbroken [same-orbitals-for-same-spin (SODS)] solution. One indication of when this occurs is where the value of the expectation value of the spin operator  $\langle \hat{S}^2 \rangle$  differs from the expected value for a triplet of  $S(S+1) = 2$ . As shown in **Fig. 6**, this occurs at a bond distance  $R = 3.7$  bohr. For larger values of  $R$ ,  $\langle \hat{S}^2 \rangle$  approaches the value of 3 which corresponds to a value of  $S = (\sqrt{13} - 1)/2 = 1.303$  which is not particularly physical. When  $R < 3.7$  bohr, no symmetry breaking occurs (i.e., we have a SODS calculation) and the PEC is the same as if no symmetry breaking at all had occurred. The exact value (also known as the Coulson-Fischer point) at which symmetry breaking occurs will depend upon the choice of density-functional. However we can expect that symmetry breaking will occur somewhere around  $R = 3.7$  bohr for most density-functional approximations (DFAs).

Before proceeding to treating the two excited  $^1O_2$  states, we need a reference state. We have noticed that demanding a multiplicity of one in many DFT programs results in the programming attempting to place the two paired electrons in the *same*  $\pi^*$  orbital which then has a higher energy than the vacant  $\pi^*$  orbital (because the filled  $\pi^*$  orbital has an erroneous self-interaction energy not present in the vacant  $\pi^*$  orbital). This results in the two paired electrons being dumped into the other, lower energy  $\pi^*$  orbital which then becomes higher in energy and so forth, with the result that calculations do not converge.

However we found easy convergence to having the two paired electrons in the same orbital in this case when we simply used the restart file from our triplet calculation and imposed a spin multiplicity of one (keyword MULTI 1). The PEC for this reference state and the BLYP DFA is shown in **Fig. 7**. Notice the uneven behavior of the reference state PEC between  $R = 3.7$  Å (the Coulson-Fischer point) and  $R = 4.1$  Å. This might be a reflection of convergence difficulties which are often encountered in the vicinity of Coulson-Fischer points. **Figure 8** shows the spin-contamination in our spin-broken reference state as a function of bond distance. The value of  $\langle \hat{S}^2 \rangle = S(S+1)$  should be zero for a singlet and two for a triplet. The value of  $\langle \hat{S}^2 \rangle$  is constant at  $S(S+1) = 1$  (corresponding to an

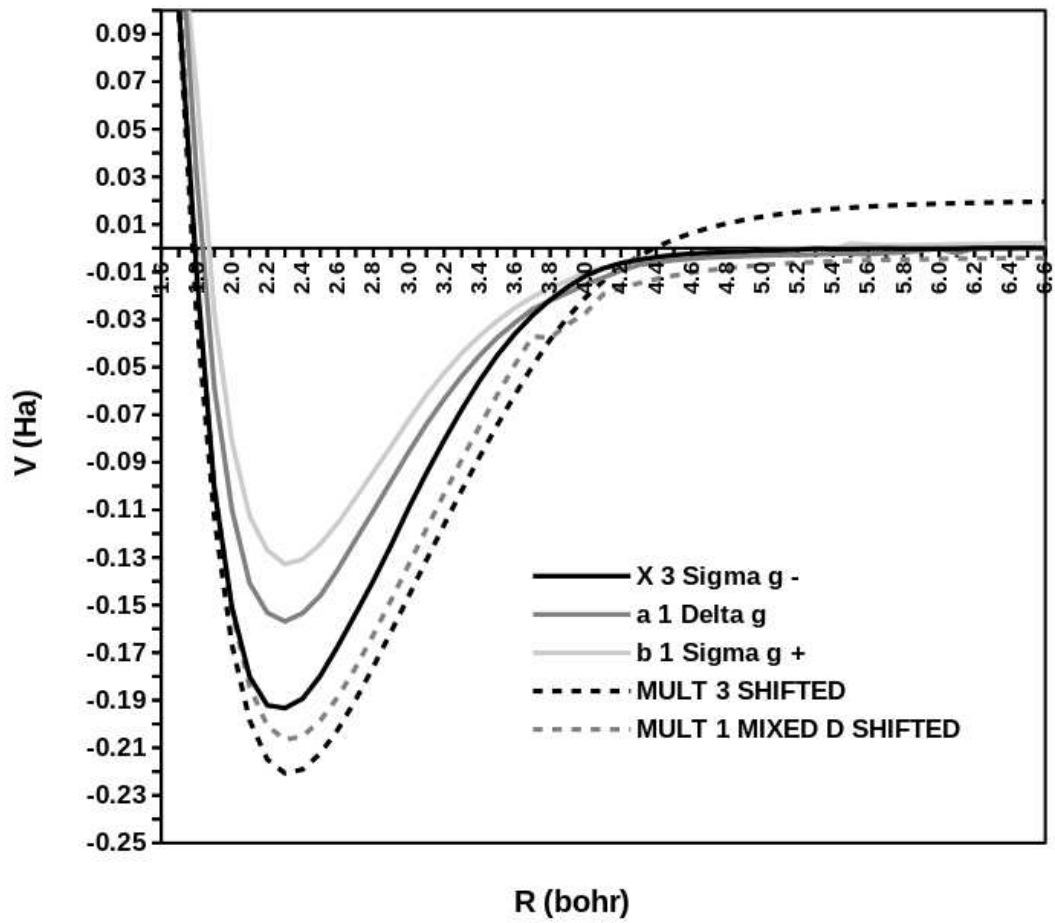


Figure 7: PEC for the  $\pi_x^*[\uparrow\downarrow]\pi_y^*$  reference state: solid lines, best estimates; black dashed line, broken symmetry triplet; grey dashed line, broken symmetry reference. Note that the labels  $\pi_x^*$  and  $\pi_y^*$  are only strictly correct when no symmetry breaking occurs.

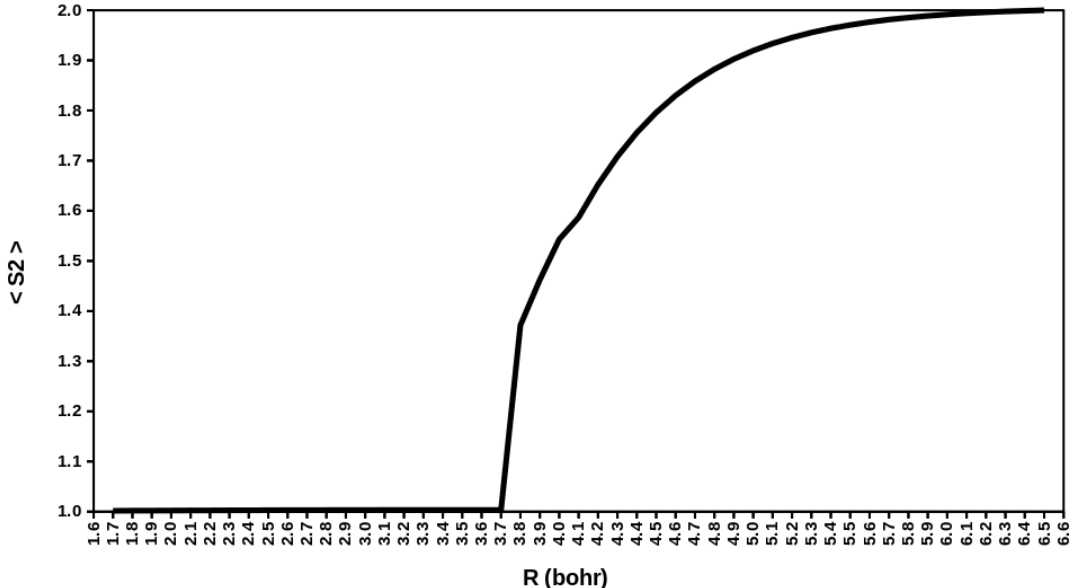


Figure 8:  $\text{O}_2 \langle \hat{S}^2 \rangle$  for the reference state in the symmetry-broken calculation.

unphysical value of  $S = (\sqrt{5} - 1)/2 = 0.6180$ ) up to the same bond length where spin contamination set in for the triplet state. It then seems to converge to a triplet state at very large values of  $R$ . While this might seem strange for a calculation which fixes one up spin and one down spin, it is perfectly consistent with the Löwdin formula [40] (Ref. [41] provides an “easy” derivation using second quantization),

$$\langle \hat{S}^2 \rangle = - \sum_{i,j} |\Delta_{i,j}|^2 + \frac{n_\alpha + n_\beta}{2} + \left( \frac{n_\alpha - n_\beta}{2} \right)^2, \quad (33)$$

because  $n_\alpha = n_\beta = 1$  and the spin-transfer matrix ( $\Delta$ ) goes to zero at large distance in this case.

We may now use this reference state to carryout a MSM BLYP DFA calculation whose results are shown in **Fig. 9**. Before the Coulson-Fischer point at  $R = 3.7 \text{ \AA}$ , there is no symmetry breaking and our calculation behaves much the same way as does the symmetry-unbroken calculations described below. Once symmetry-breaking sets in, the calculation is no longer straightforward. In particular, one of the problems that we encountered in doing broken-symmetry MSM calculations is that the spin  $\alpha = \uparrow$  MOs do not always correspond exactly with the spin  $\beta = \downarrow$  MOs. Usually this is just a matter of a reversal of orbital numbering. However it could be more complicated and this inexact correspondance (together with the aforementioned difficulties with the ground  $X^3\Sigma_g^-$  state calculation) could explain the uneven behavior of the PECs between  $R = 3.7 \text{ \AA}$  (the Coulson-Fischer point) and  $R = 4.1 \text{ \AA}$ . Nevertheless we do obtain the correct ordering of *singlet states* at large distance even though our results are certainly *not* quantitatively correct and the triplet state lies incorrectly between the two singlet states. Of course, the most important difficulty and *the most important reason to avoid symmetry breaking when treating excited states* is that it is nearly impossible to construct excited states with well-defined symmetries unless the molecular orbitals belong to well-defined irreducible representations of the molecular point group, which is certainly not the case in broken-symmetry (DODS) calculations. Henceforth we consider only symmetry-unbroken (SODS) calculations.

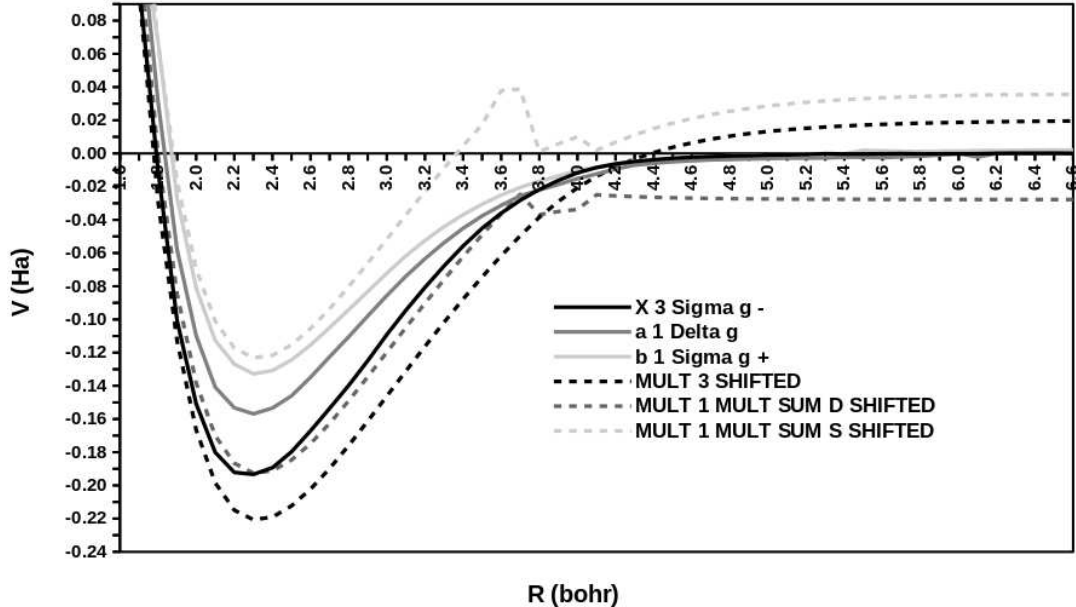


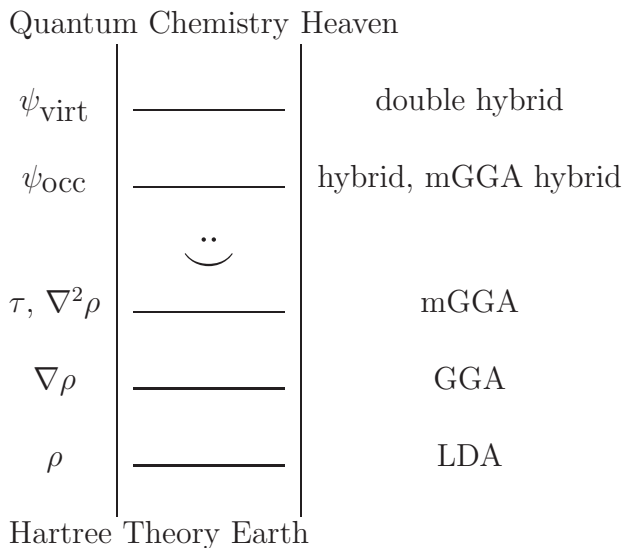
Figure 9: Comparison of  $O_2$  MSM BLYP PECs from our symmetry-broken calculation (dashed lines) with best estimate PECs (corresponding solid lines).

### 4.3 No Symmetry Breaking

We have calculated the PECs for the  $X^3\Sigma_g^-$  ground state, the  $a^1\Delta_g$ , and the  $a^1\Sigma_g^+$  singlet excited states using the MSM and various DFAs. As already explained in Sec. 2, our general procedure is to first construct a reference state with half a spin  $\alpha = \uparrow$  electron and half a spin  $\beta = \downarrow$  electron in each  $\pi^*$  orbital and then reoccupy the resultant orbitals to create the single-determinantal states (including that for the ground  $X^3\Sigma_g^-$  state) needed for the MSM calculation. Otherwise the procedure is very similar to that described in the previous subsection where symmetry breaking was discussed. Our major focus will be on the behavior of different *functionals* (DFAs) in MSM calculations of the first three electronic states of  $O_2$ . The ground  $X^3\Sigma_g^-$  state will be treated more summarily as the quality of ground-state properties have been extensively studied as a function of choice of DFA. Our main interest is in the choice of DFA for describing the two  $^1O_2$  excited states using the MSM method as very little seems to be known about this.

Although repetitive for DFT experts, it seems appropriate to begin with a very brief reminder of the various rungs of the Jacob’s ladder of DFAs shown in **Table 3**. The basic idea is that we climb the ladder by allowing our exchange-correlation energy functional to depend on more and more variables. This typically requires us to calculate more complicated quantities, making more resource-intensive calculations, but is not guaranteed to give better results. However there is a tendency for functionals from higher rungs of the ladder to be more accurate than those from lower rungs of the ladder (see, e.g., Ref. [44]). The lowest rung is the local (spin) density approximation (LDA) where the exchange-correlation (xc) energy density at each point in a molecule only depends upon the density at that point in the molecule. The next level is constituted by the generalized gradient approximations (GGAs) where the xc energy density depends also on the gradient of the density at that point. Meta GGAs (mGGAs) go a step further by including either an orbital dependence through the kinetic energy density  $\tau$  or via the Laplacian of the density. Hybrid functionals include some contribution from the exact (also known as Hartree-Fock) exchange as well as GGA exchange and correlation. In

Table 3: John Perdew’s vision of a Jacob’s ladder for DFAs [42, 43]. On the left of the ladder are the new variables which may be used to make functionals once that rung is reached. On the right is the name usually given to that level of approximation. In the middle is a user drawn as an angel in the smiley (emoji) approximation. The user needs to be able to ascend and descend the ladder in search of the right compromise between accuracy and computational resources to meet his or her needs.



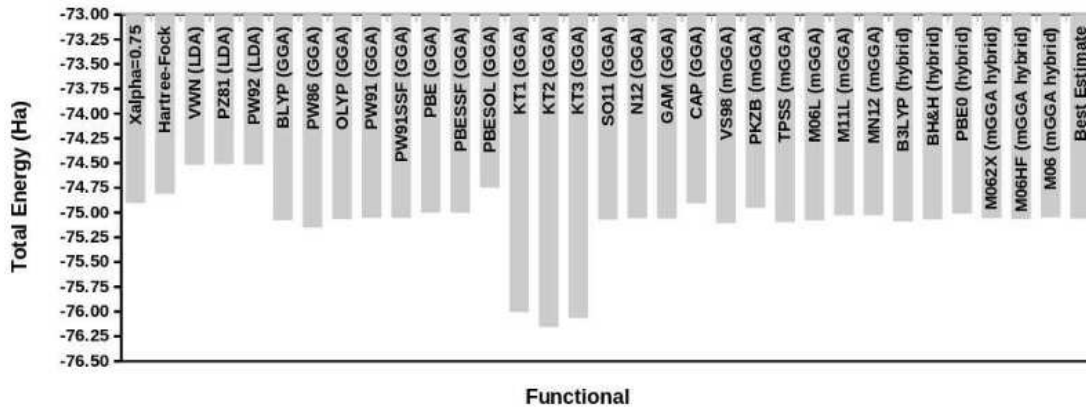
DEMON2K, there are also hybrid functionals which are constructed using mGGAs.

So much has been learned for the various levels of Jacob’s ladder for ground-state calculations that must already be familiar to most users of DFT, that we do not want to belabor our comparison of DFAs. However we do need to recall a few things about what is known from ground state calculations before commenting on MSM DFT excited-state calculations.

**Figure 10** compares calculations of the total electronic energy of the  $O(^3P)$  atom. This quantity is needed in order to evaluate the energy of the  $O_2$  chemical bond in the three electronic states. The  $X\alpha$  method was designed to behave like Hartree-Fock (HF) which gives too high an energy because of the lack of electron correlation. Perhaps surprisingly the three LDA parameterizations over-estimate the atomic energies even worse than do  $X\alpha$  and HF (leading to overbinding in molecules). The GGAs, mGGAs, hybrids, and mGGA hybrids lead to substantial improvements over the LDA ( $X\alpha$ ) and HF with, some notable exceptions such as PBESOL which was specifically parameterized to treat solids and the KT1, KT2, and KT3 functionals which were originally intended for nuclear magnetic resonance (NMR) calculations. Only 5 GGAs (OLYP, PW91, PW91SSF, N12, and GAM), one hybrid (BH&H), and two mGGA hybrids (M062X and M06HF) are within an arbitrary cut-off of  $0.2 \text{ eV} = 0.00735 \text{ Ha}$  of our best estimate value.

It is often said that quantum chemistry works by error cancellation. That is, that errors in the energy of core electrons cancel out when chemical bond energies are calculated. This is why atomic  $O(^3P)$  energies are not as important as the bond energies shown in **Fig. 11**. Before John Perdew spoke of Jacob’s ladder, Axel Becke had already spoken of the three generations of DFAs. In Becke’s scheme,  $X\alpha$  and Hartree-Fock (HF) were pre-history. We found severe underbinding of  $O_2$  at the HF level with respect to twice the energy of  $O(^3P)$ . But this is the only functional where we see this problem.  $X\alpha$  was supposed to be parameterized to behave like HF but actually behaves more like

(a)



(b)

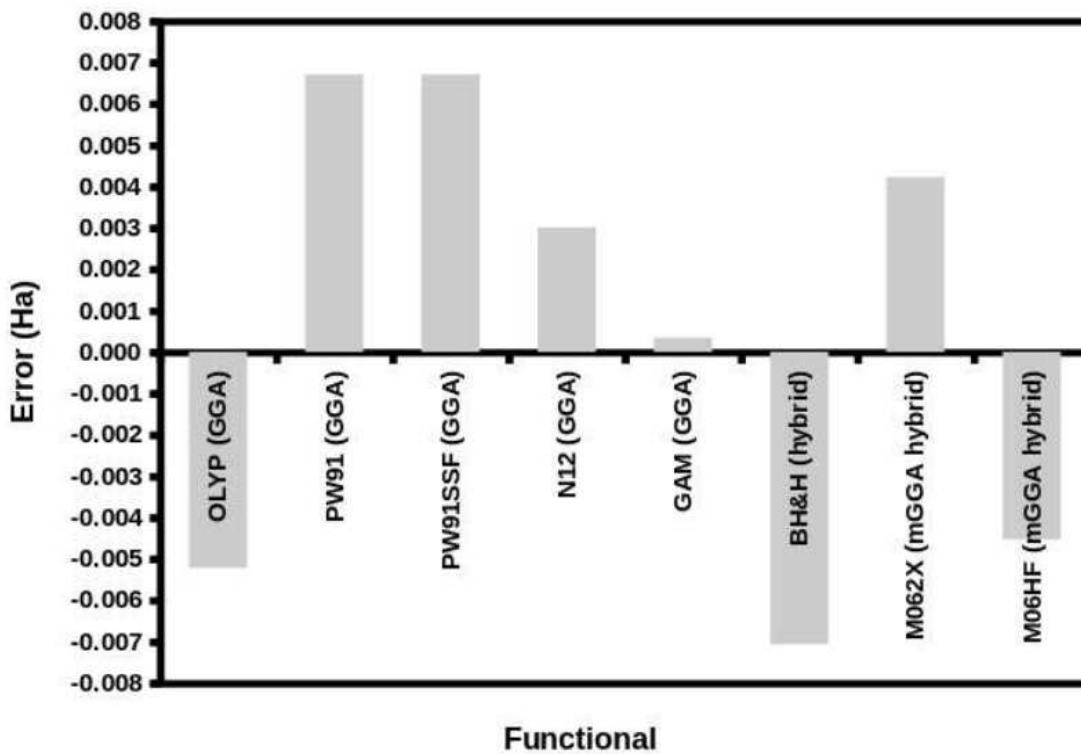
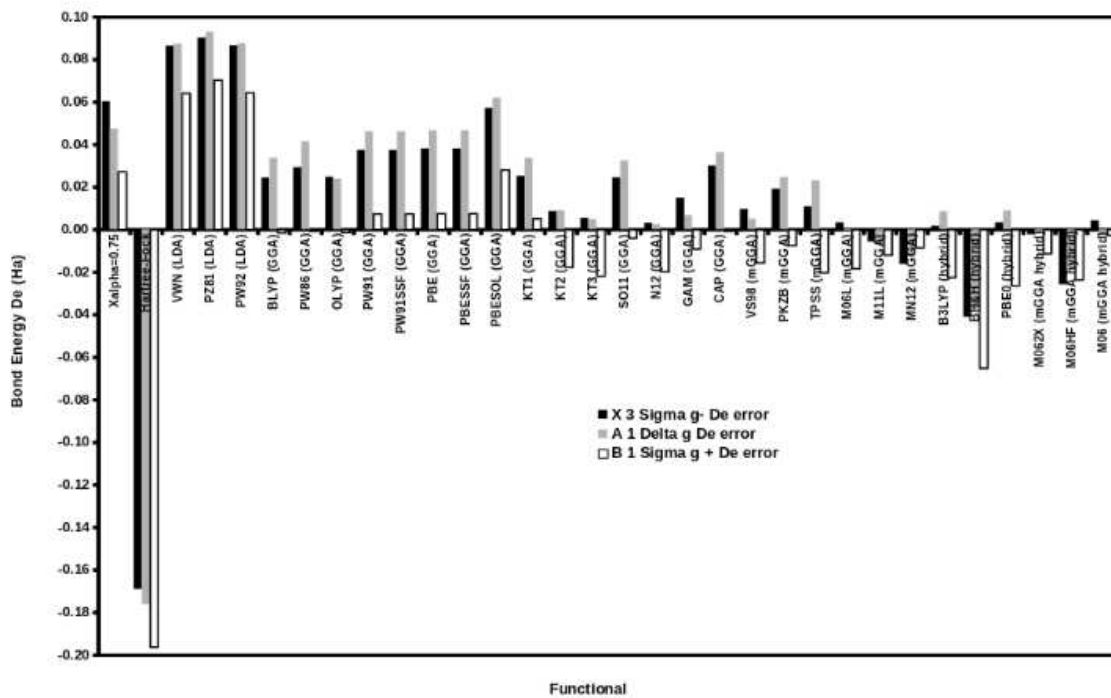


Figure 10: Comparison of total  $O(^3P)$  atomic energies calculated with various DFAs: (a) total energies, (b) functionals with an absolute error of less than 0.2 eV with respect to the best estimate for the  $O(^3P)$  atomic energy taken from Ref. [45].

(a)



(b)

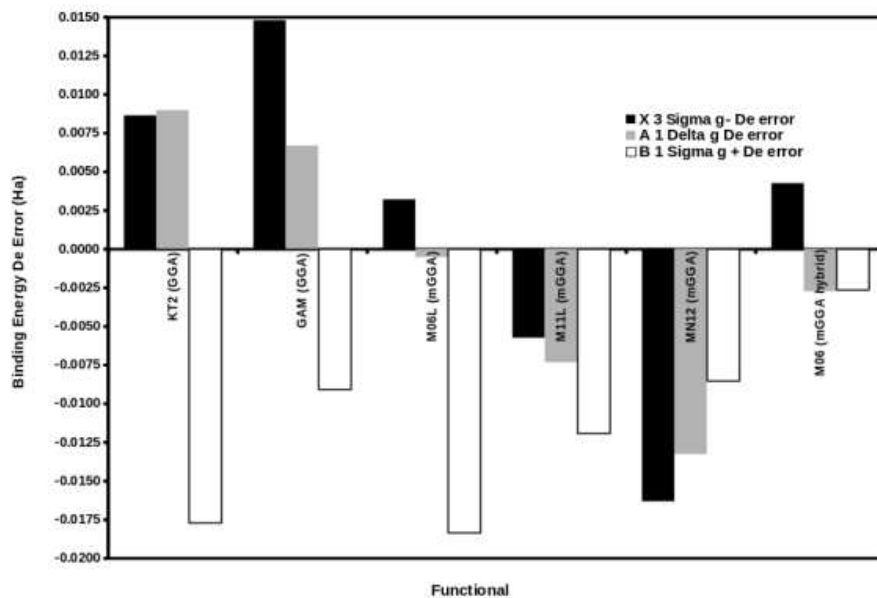


Figure 11: Comparison of the binding energy,  $D_e = 2E(O(^3P)) - E(O_2)$ , calculated with various DFAs: (a) error with respect to the best estimate, and (b) zoom in on functionals showing the smallest errors. The best estimate is from Fig. 1 of Ref. [20]. (See the *Supplementary Information* for a table binding energies.)

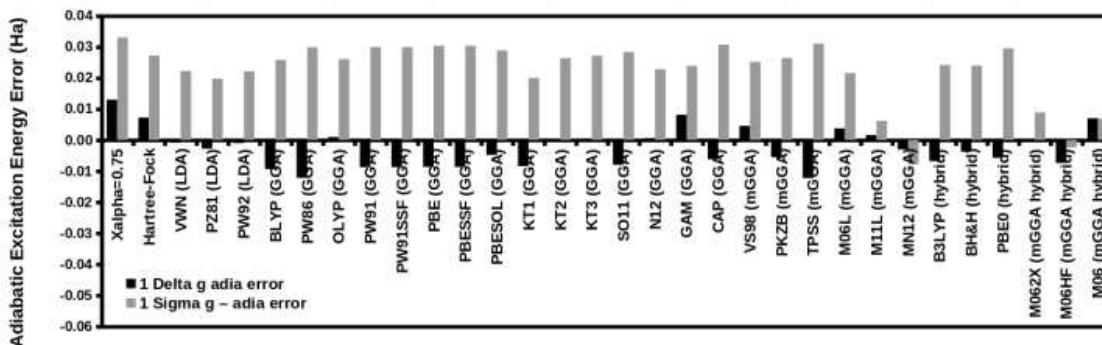
the LDA. Becke’s first generation is that of the LDA which was known to overbind molecules. As we have seen in the case of  $O_2$ , this is because the LDA energy of  $O(^3P)$  is too high in energy. The second generation is that of the GGAs which did much to correct the overbinding problem and make DFT useful for chemical applications. However GGAs could not yet approach chemical accuracy (defined as 1 kcal/mol = 0.001594 Ha). Only the third generation — namely hybrid functionals — could approach this level of accuracy. All of this is well-known for the ground state. However we now see that the same holds for the bond energies obtained for the  $a^1\Delta_g$  excited state. Oddly enough most functionals give relatively small *absolute* errors for the  $b^1\Sigma_g^+$  state. However this is actually a bad thing as for most applications we are interested in the energy of the  $b^1\Sigma_g^+$  state relative to the  $X^3\Sigma_g^-$  and  $a^1\Delta_g$  state. Choosing an arbitrary cut-off of 0.02 Ha = 0.544 eV = 12.6 kcal/mol, we find that only two GGAs (KT2 and GAM), three mGGAs (M06L, M11L, and MN12), and one mGGA hybrid (M06) are able to obtain absolute energies to within this error range of our best estimate for the bond energies of all three states.

A more delicate test of energetics is to calculate excitation energies. Vertical excitation energies are the difference of electronic energies of the excited states and the ground state at the equilibrium geometry of the ground state, whereas adiabatic excitation energies are the difference of electronic energies of the excited states and the ground state at the equilibrium geometry of the ground state. As such, adiabatic excitation energies are the difference of the bond energies in the ground  $^3O_2$  state and the two excited  $^1O_2$  states. Both types of excitation energies are tabulated in the *Supplementary Information*. Here, for a reason which will be explained below, we will focus on adiabatic excitation energies (**Fig. 12**). It is evident that accurate  $a^1\Delta_g$  excitation energies are fairly easily calculated using the MSM method. This means that it is fairly easy to obtain a reasonably accurate spin-flip energy  $F$ . In contrast, most functionals significantly over-estimate the  $b^1\Sigma_g^+$  excitation energy, meaning that the spin-pairing energy  $P$  is overestimated. There are four exceptions which stand out as being notably better in this respect, namely two mGGA (M11L and MN12) and three mGGA hybrid (M062X, M06HF, and M06) functionals. We have already noted that there is a scarcity of MSM DFT results for  $^1O_2$  with which to compare but have already presented a comparison of the results that we have found with some of our results in Table 1. These have already been discussed in the introduction. A puzzling point is why our M06HF/DEF2-TZVPP MSM results (see the excitation energies in the *Supplementary Material*) are so different from the MSDFT/M06HF/cc-pVTZ results reported in Ref. [19]. We think that this might be due to confusion between the M062X, M06HF, and M06 mGGA hybrid DFAs which were all presented in the same reference [46] as our M06/DEF2-TZVPP MSM results certainly do resemble the MSDFT/M06HF/cc-pVTZ results reported in Ref. [19].

Some time ago, one of us (MEC) was involved in an extensive series of studies comparing DFAs for calculating the  $^5T_{2g} : (t_{2g})^4(e_g)^2 - ^1A_{1g} : (t_{2g})^6(e_g)^0$  spin-crossover energy difference in octahedral Fe(II) complexes [47, 48, 49, 50, 51]. An important conclusion of these studies is that HF would tend to stabilize the configuration  $\pi_x[\uparrow\downarrow][\ ]\pi_y$  more than would the LDA or GGAs with respect to the configuration  $\pi_x[\uparrow][\uparrow]$ . That is, HF should underestimate the spin-pairing energy  $\tilde{P} = E(\pi_x[\uparrow\downarrow][\ ]\pi_y) - E(\pi_x[\uparrow][\uparrow])$  while the LDA and GGAs tend to overestimate  $\tilde{P}$ . We also found that the OLYP functional tended to give a less severe overestimation. This is confirmed in **Fig. 13**. Note that  $\tilde{P} \neq P$  represent two different pairing energies.

Returning again to the problem of octahedral Fe(II) spin-crossover complexes, it has been argued [52] that the real problem lies not with the total exchange-correlation energy but with the accuracy of the exchange-correlation potential which is unable to produce an accurate enough density. They show that the problem disappears when an accurate density is used in the xc energy functional rather than a self-consistent density. Although we find this to be an interesting discovery, we have

(a)



(b)

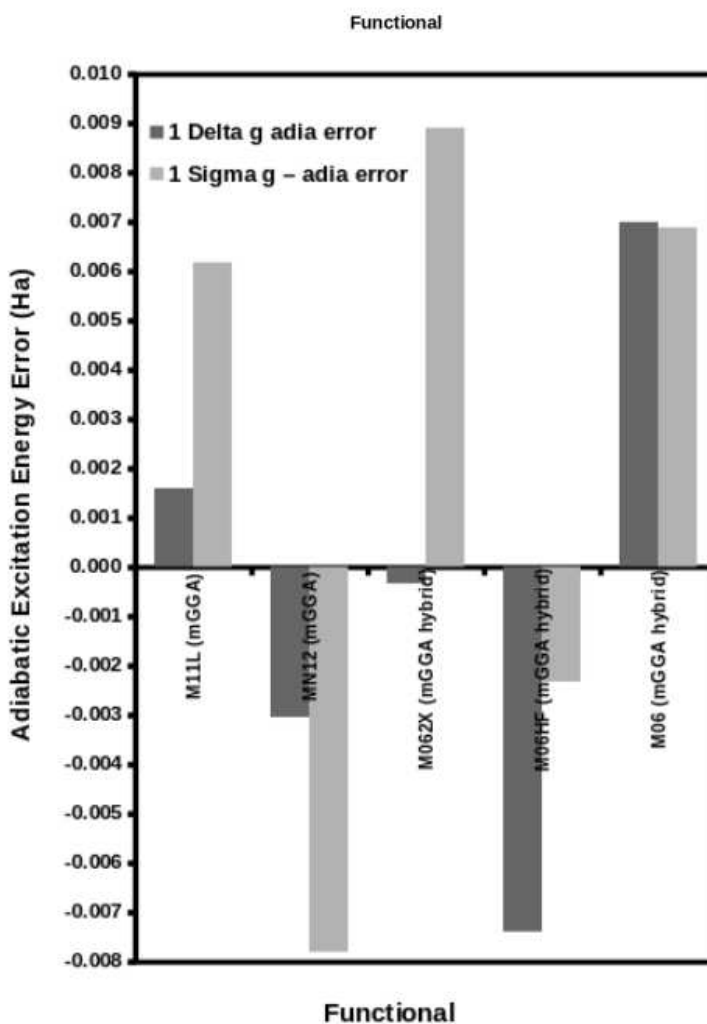


Figure 12: Comparison of the singlet adiabatic excitation energies  $\Delta E = D_e(^3O_2) - D_e(^1O_2)$  calculated with various DFAs: (a) error with respect to the best estimate, and (b) zoom in on functionals showing the smallest errors. The best estimate is from Fig. 1 of Ref. [20].

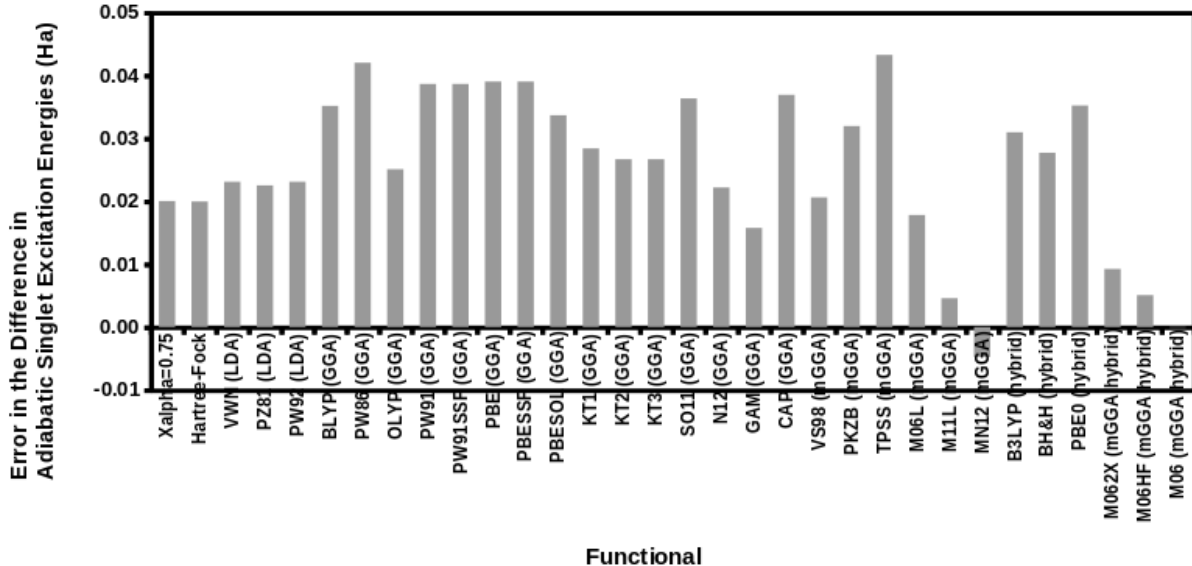


Figure 13: Comparison of the error in twice the pairing energy  $2\tilde{P} = E[b^1\Sigma_g^-] - E[a^1\Delta_g]$  calculated with various DFAs.

not pursued it for the present problem.

#### 4.4 Shape of the Multiplet Sum Method Surfaces

Thus far we have focused mainly on energy differences (namely bond energies and excitation energies). We now wish to go further and discuss the shape of the PECs. As the  $^3\text{O}_2$  ground state and the two  $^1\text{O}_2$  excited states differ only by a redistribution of the two  $\pi^*$  electrons, it might be anticipated that the  $X^3\Sigma_g^-$ ,  $a^1\Delta_g$ , and  $b^1\Sigma_g^+$  PECs should all have roughly the same shape. However further reflection shows that this cannot occur if they have different bond energies ( $D_e$ ) and the same dissociation limit. There must be some state-dependent shape differences and the question arises as to what extent this is reflected in our DFT MSM calculations. All our MSM curves are derived from the same reference state with half a spin  $\alpha = \uparrow$  and half a spin  $\beta = \downarrow$  electron in each  $\pi^*$  orbital. Once upon a time, such a state would have been indistinguishable from the ground state because exchange-correlation energy functionals had no spin dependence. However that was a long time ago. Nevertheless we might expect that the different PECs should behave something like the ground  $X^3\Sigma_g^-$  PEC, particularly since no additional self-consistent field (SCF) cycles are carried out after reoccupying the orbitals of the reference state. This is indeed what is seen in the graphs shown in the *Supplementary Information*. But let us take a closer look.

**Figure 14** confirms that the MSM DFT bond lengths with a given functional seem to be roughly independent of the electronic state. This is in contrast with the experimental observation [20, 32] that the higher-energy electronic states which have smaller bond energies also have longer bond lengths. Moreover, the functionals which were previously found to be optimal for energies are not the ones found to give the best bond lengths.

Let us turn next to the curvature at the bottom of the PEC wells as measured by the harmonic frequency. As may be expected from the above discussion of symmetry-broken and symmetry-unbroken problems and from the graphs in the *Supplementary Information*, our symmetry-unbroken

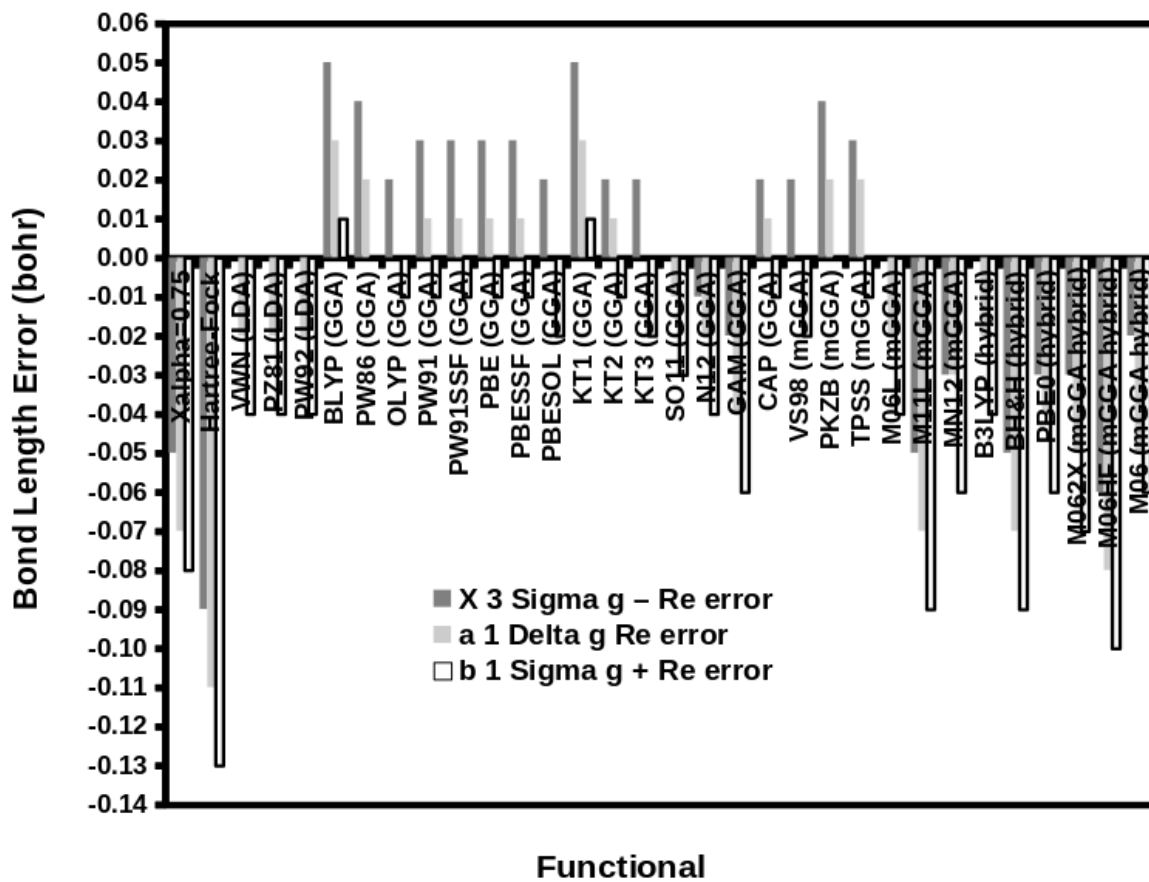


Figure 14: Bond distances calculated with various DFAs compared with best estimate values from Refs. [20, 32]: error in the distance with respect to Ref. [32].

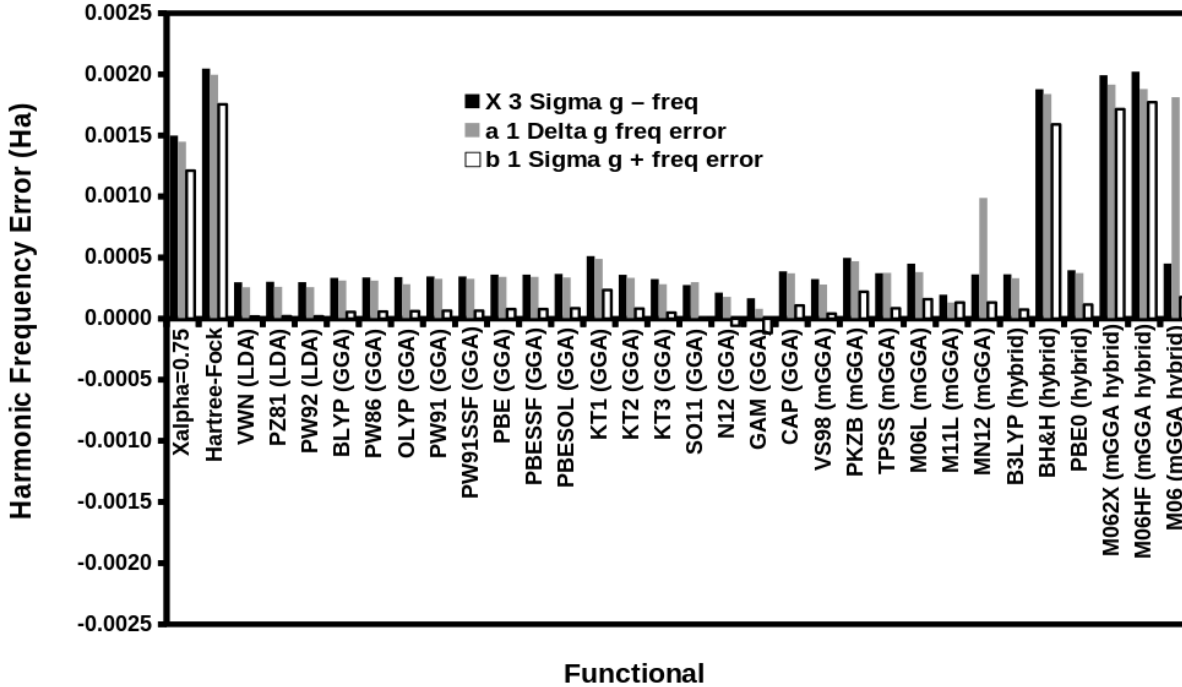


Figure 15: Harmonic frequencies calculated with various DFAs compared with best estimate values from Refs. [20, 32]: error in the frequency with respect to values from Ref. [20].

PECs are expected to be significantly more parabolic,

$$V(R) = \frac{k}{2} (R - R_e)^2 + \text{HOT}, \quad (34)$$

than the best estimate PECs. Here “HOT” stands for “higher-order terms.” To find  $k$  and  $a$ , we fit three points around the minimum to the quadratic,

$$V(R) = AR^2 + BR + C. \quad (35)$$

Then  $A = k/2$ . Also from the classical mechanics of a simple harmonic oscillator,  $k = \mu\omega_0$ , where the reduced mass  $\mu = m^2/(m + m) = m/2$  in terms of the actual mass of an oxygen atom  $m = M/N_A = (15.999 \text{ g/mol})/(6.022 \times 10^{23}/\text{mol}) = 2.6568 \times 10^{-23} \text{ g} = 29165 m_e$ . So

$$\hbar\omega_0 = 2\sqrt{\frac{A}{m}}. \quad (36)$$

Harmonic frequencies are shown in **Fig. 15** (and numbers are tabulated in the *Supplementary Information*). We might expect the harmonic frequencies to decrease as we go to higher-energy states because the PEC well is becoming shallower and this is indeed what is seen in the experimental data of Ref. [32]. However the effect is small and we do not see it in the harmonic frequencies extracted from Fig. 1 of Ref. [20]. The LDA is famous for giving good harmonic frequencies (due to error cancellation) and this is clearly seen in Fig. 15. That we also see this for the LDA, GGAs, and mGGAs, both for the ground and for the two excited states is very reassuring. Less reassuring are the relatively large errors seen for the MN12 mGGA and for the M06 mGGA hybrid for the  $a^1\Delta_g$  state and for all the states for the BH&H hybrid, the M062X mGGA hybrid, and the M06HF hybrid.

We may also estimate anharmonicities by assuming that the PECs may be approximated, at least roughly, by a Morse potential [53],

$$\begin{aligned} V(R) &= D_e e^{-(R-R_e)} (e^{-a(R-R_e)} - 2) \\ &= D_e [a^2 (R - R_e)^2 - 1] + \text{HOT} \end{aligned} \quad (37)$$

As the Schrödinger equation may be solved exactly for a Morse potential to obtain,

$$\begin{aligned} E_n &= \hbar\omega_0 \left( n + \frac{1}{2} \right) - \frac{[\hbar\omega_0 (n + \frac{1}{2})]^2}{4D_e} \\ &= \hbar\omega_0 \left( n + \frac{1}{2} \right) + \hbar x_0 \omega_0 \left( n + \frac{1}{2} \right)^2, \end{aligned} \quad (38)$$

we may also obtain the anharmonicity from the bond energy and harmonic frequency as,

$$\hbar x_0 \omega_0 = \frac{\hbar^2 \omega_0^2}{4D_e}. \quad (39)$$

For completeness, we note that,

$$a = \frac{\omega_0}{2} \sqrt{\frac{m}{D_e}}, \quad (40)$$

in the Morse equation so that we may plot the PECs. According to Eq. (39), the anharmonicity is determined by the harmonic frequency and by the bond energy. **Figure 16** shows that the best functionals for calculating the anharmonicity are also pretty much the best ones for calculating the harmonic frequency.

The question now arises as to how to choose the best functional for DFT MSM calculations. There are, in fact, two questions: (a) “What functional is best for a random unknown molecule?” and (b) “What functional is best for O<sub>2</sub>?” Clearly we can only answer question (b) and even in that case, it depends upon making choices and compromises between the shapes of the PECs and their absolute or relative energies. **Figure 17** shows the Morse curves obtained from the MSM with the M06 GGA which seems to be a fair compromise between competing interesting features of the PECs, albeit one which places more emphasis on absolute energies than upon other factors.

## 5 Conclusions and Perspectives

Twenty percent of our atmosphere is made up of molecular oxygen, which is nearly all in the ground  $X^3\Sigma_g^-$  state. Some of this relatively kinetically-unreactive triplet molecule ( $^3\text{O}_2$ ) is constantly being converted into the very reactive singlet form ( $^1\text{O}_2$ ). Understanding how this happens, how to take advantage of  $^1\text{O}_2$  to carry-out desired reactions, and how to get rid of  $^1\text{O}_2$  to avoid undesirable reactions involves understanding how  $^1\text{O}_2$  reacts with large molecules, such as C<sub>60</sub>. The size of these molecules tends to rule out the use of sophisticated, accurate, yet computer-resource intensive, *ab initio* methods in favor of the computationally simpler density-functional theory (DFT) approach. But it is this very simplicity which should act as a warning when applying DFT to intrinsically-multideterminantal problems such as open-shell systems, excited states, and the calculation of potential energy curves (PECs) that involve the making and breaking of bonds.

Hohenberg-Kohn-Sham DFT [54, 55] assumes the existence of a fictitious system of noninteracting electrons whose ground-state charge density is the same as that of the real system of interacting electrons. This is the assumption of noninteracting *v*-representability which does not always hold [37],

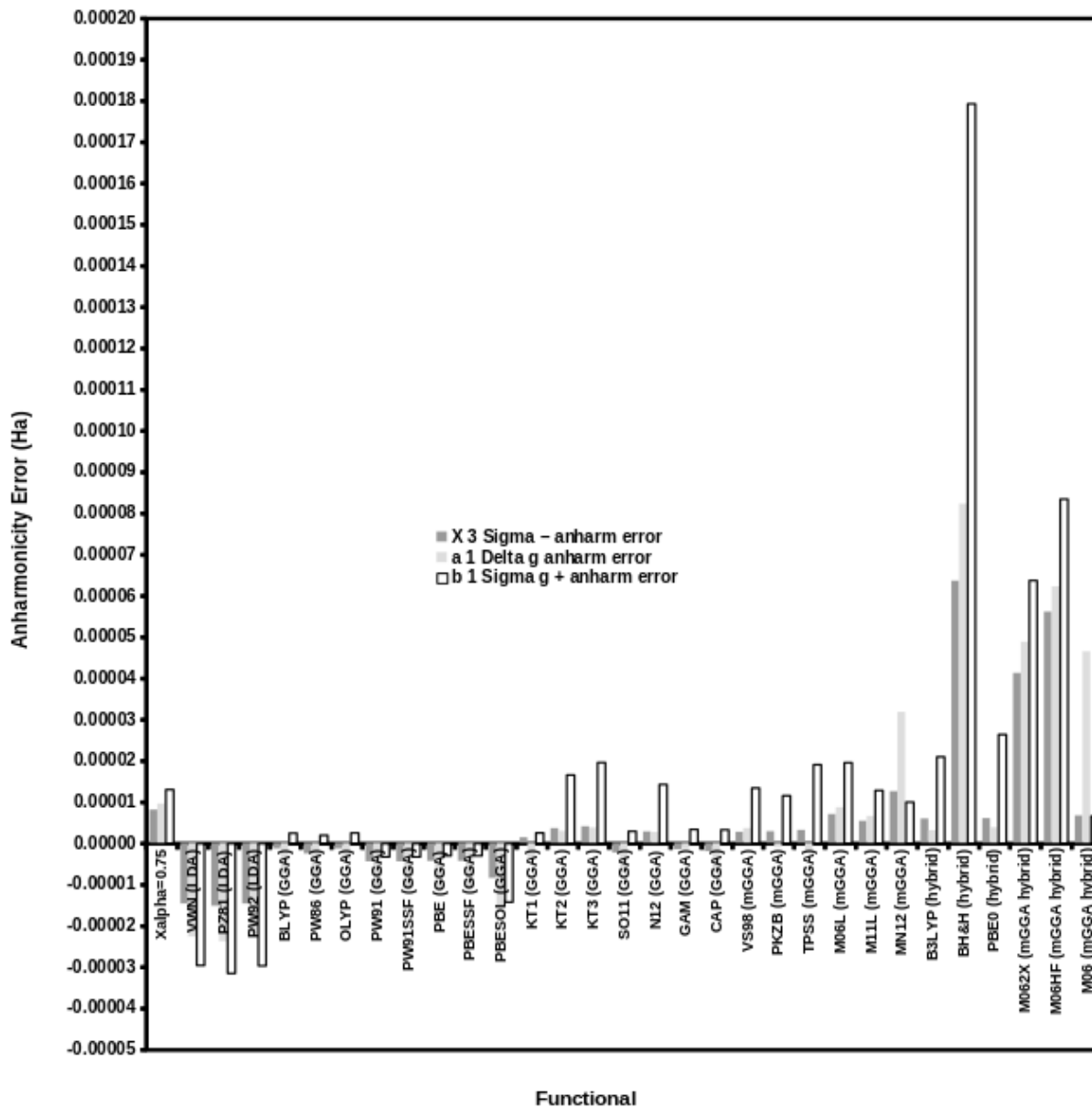


Figure 16: Anharmonic frequency corrections calculated with various DFAs compared with best estimate values from Refs. [20, 32]: error in the anharmonic correction with respect to values from Ref. [20] (except for HF which shows much larger errors).

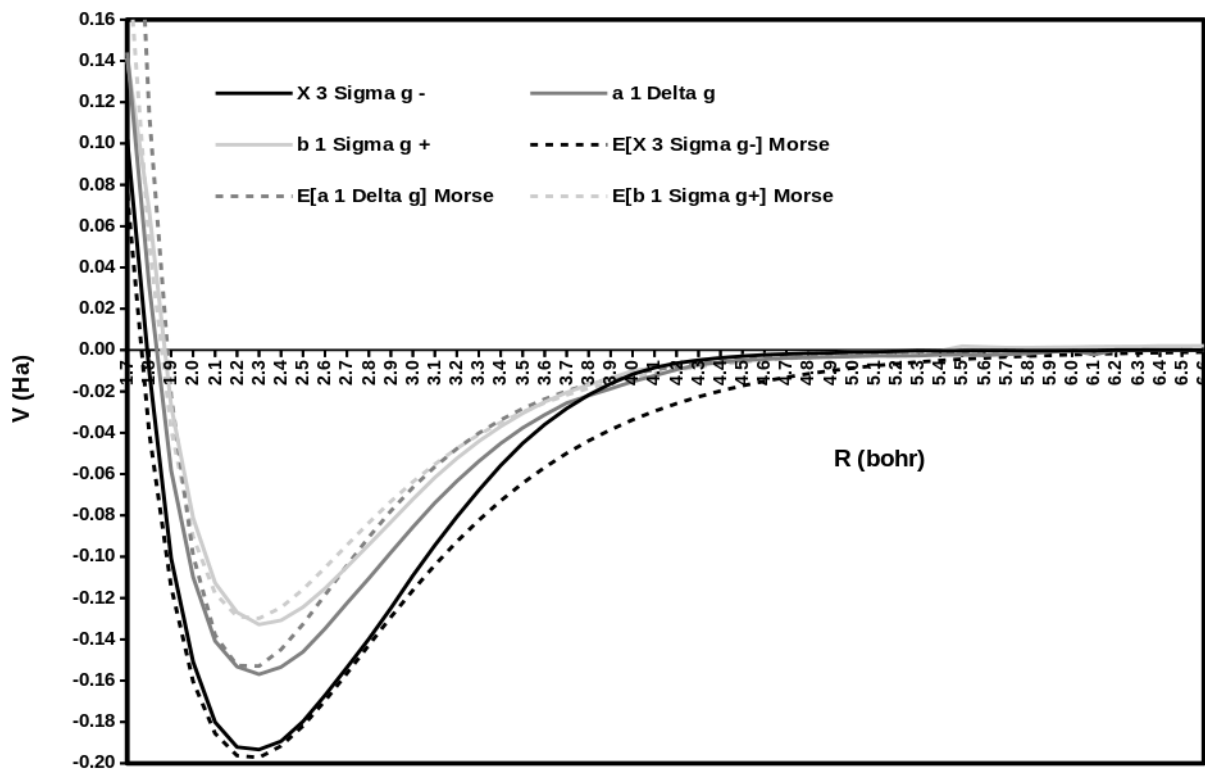


Figure 17: Comparison of the Morse potential calculated using data obtained via MSM calculations with the M06 GGA and best estimate PECs from Ref. [20].

particularly in strongly multideterminantal situations such as open-shell molecules or when bonds are being made or broken. Requiring effective noninteracting  $v$ -representability of an approximate density functional means placing particularly difficult demands on density-functional approximations (DFAs) as it means that we expect them to be able to model the behavior of an intrinsically multideterminantal wave function, which even the exact functional might not be able to model, using only a single-determinantal Kohn-Sham wave function. This is why the Ziegler-Rauk-Baerends-Daul [6, 7] multiplet sum method (MSM) proposes an alternative way of treating intrinsically multideterminantal systems by using symmetry to deduce equivalent energy expressions involving only single-determinantal energy expressions. This method is widely used to treat open-shell singlet excited states.

We have shown that the  $a^1\Delta_g$  state of  $^1\text{O}_2$  may be treated using exactly the same DFT MSM approach used for open-shell singlet excited states. Oddly enough this does not seem to be widely known (or at least we have been able to find at most one other reference using something like this approach for  $^1\text{O}_2$  [19]). We speculate that this might be due to the large amount of confusion in the photochemical literature regarding the proper molecular orbital picture of the  $^1\text{O}_2$  excited states combined, perhaps, with little or no overlap between the transition-metal complex and magnetic property communities most likely to use the DFT MSM approach and the community interested in  $^1\text{O}_2$  photosensitizers. Furthermore, we point out that the DFT MSM may also be used to obtain the  $b^1\Sigma_g^+$  state of  $^1\text{O}_2$ .

The main limitation is that the symmetry analysis underlying the MSM and the labeling of states in small molecules is incompatible with the symmetry-breaking different-orbitals-for-different-spins (DODS) method typically used to study PECs over a broad range of bond distances. Instead we have made an extensive study of the behavior of the DFT MSM for describing PECs in the region close to the equilibrium bond length where no symmetry breaking occurs. We found good  $a^1\Delta_g$  excitation energies with most functionals but that obtaining accurate ground- and excited-state bond energies and a good  $b^1\Sigma_g^+$  excitation energy requires us to climb the Jacob’s ladder of functionals to rungs using mGGAs and mGGA hybrid functionals. Unfortunately this is also accompanied by some degradation of the quality of bond lengths and harmonic frequencies. Nevertheless it is possible to obtain reasonable approximate PECs for all three states ( $X^3\Sigma_g^-$ ,  $a^1\Delta_g$ , and  $b^1\Sigma_g^+$ ) by the use of a Morse potential extrapolation to longer bond lengths. Although a somewhat arbitrary choice, we illustrated how this works with the M06 functional.

This brings us to the point of how to move beyond the MSM to be able to apply DFT-based methods to increasingly complicated photochemical systems. Some readers may recognize that one of the authors (MEC) was a pioneer in the formulation of time-dependent (TD) DFT for treating excited states in quantum chemistry [56] (see also the reviews in Refs. [57, 37]). An obvious problem with the MSM is that it relies too much on symmetry to estimate the trial wave function which makes it difficult to apply to larger, less symmetric systems. The MSM also requires human intervention to choose the reference system and the configurations to be treated. In this sense, the MSM resembles multiconfigurational wave function methods such as the complete active space (CAS) self-consistent field (SCF) method. In contrast TD-DFT provides a fully automatic procedure for treating excited states which meshes nicely with algorithms already needed in DFT programs to evaluate gradients and response properties. This, and its good performance to computer resource ratio, is one of the reasons that TD-DFT has become a major tool in the quantum chemistry toolbox.

But it would be very wrong to think that TD-DFT replaces the MSM. Indeed MEC has always found it remarkable that, though the MSM and TD-DFT are based upon very different formalisms, they typically give very similar answers *in situations where both apply*, which typically means (for TD-DFT) situations where the ground state is reasonably well described by a single determinantal

wave function and excitations are limited to energetically low-lying localized states with little or no relaxation of the charge density and (for the MSM) there is a good reference state and enough symmetry relations may be deduced to reduce state energies to weighted sums of single determinantal energies. It is particularly fascinating that the TD Hartree-Fock (HF) Tamm-Dancoff approximation (TDA) and  $\Delta$ SCF (HF) energy expressions, neglecting relaxation, are identical, but that this same statement is not true for TD-DFT and the  $\Delta$ SCF DFT method. Early work to reconcile these two methods was reported in Refs. [58] and [59]. It has been continued in some lovely creative work on constricted variational DFT (CV-DFT) [60, 61] that originated in the group of Ziegler (now deceased).

Given that the MSM and TD-DFT approaches are not as independent as they might seem, that both methods (and combinations thereof) are continuously evolving, and that a conclusion is a good place to give a few perspectives for the future but is *not* the proper place for a review, then we will try to limit our perspectives primarily to how the MSM method has been improved for applications to more complex problems. Nevertheless we cannot resist pointing out that, beginning with early work on TD-DFT (often with DEMON2K) for open-shell systems [62, 63, 64, 65, 41], spin-flip TD-DFT [66, 67, 68, 69, 70, 71], and dressed TD-DFT [72, 73, 74, 75, 76], progress is also being made towards a more versatile TD-DFT able to handle more complex photochemical problems. [The list of cited references is grossly incomplete, but (as said above) this is no place for a review!] Particularly relevant to the present paper is the work of Guan *et al.* applying TD spin-flip DFT to the excited-state PECs of O<sub>2</sub> [77].

Let us now return to and focus specifically on evolutions of the MSM. The natural evolution is to expand the active space and use MSM *and other* techniques to evaluate the matrix elements of a small configuration interaction (CI) problem. Historically MSM practitioners would use symmetry to write down as many relations as possible and attempt to express all needed CI matrix elements in terms of single-determinantal energies. When this was not possible, then a few additional electron repulsion integrals (ERIs) would be evaluated explicitly using the DFT orbitals. In recent years, some new tricks have been added and the resultant improved MSM goes by names like multistate DFT (MSDFT) and constrained DFT configuration interaction (CDFT-CI). Let us try to give the gist of these two methods. Both methods seem to be inspired to some extent by Marcus' theory of charge transfer and, in particular, resemble the creation of configuration mixing of delocalized (adiabatic) states from noninteracting localized (diabatic) states. The relation with the MSM enters almost accidentally and with little or no discussion.

In MSDFT [78, 79, 17, 80, 81, 82, 19], also called valence-bond DFT (VBDFT) [78], the diabatic states are based upon reactant and product orbitals and coupling is based upon arguments similar to Marcus-Hush theory [78]. The MSM was introduced in Ref. [80] in order to be able to handle spin multiplets and was also used in subsequent papers (such as Ref. [19]).

CDFT-CI comes from the group of Van Voorhis [83, 84, 85, 86, 87]. It makes no reference to the MSM, but nevertheless bears a strong resemblance to MSDFT. CDFT-CI applies a constraint to localize spin and changes on user-defined parts of the system which may not otherwise be very well described by DFT. Diagonal elements of the CI matrix are (single-determinantal) DFT energies from the constrained states and off-diagonal elements are obtained by an essentially exact expression obtained using the constraining potential. This method is implemented in DEMON2K [88, 89, 39].

So, in our O<sub>2</sub> case, the two  $\pi^*$  orbitals could be considered as subsystems to which the constraints should be applied (though this to our knowledge has never yet been tried). It should then be possible to go further and use either MSDFT or CDFT-CI (or both) to consider what happens when <sup>1</sup>O<sub>2</sub> reacts with a molecule (such as C<sub>60</sub>). Of course the presence of the molecule will lead to the loss of degeneracy of the  $a^1\Delta_g$  state and we could then begin to test the empirical rules given by Kearns

(p. 414 of Ref. [1]) for  $^1\text{O}_2$  reactions and the qualitative ways of thinking about diradical reactions advocated by Hoffmann and coworkers [34]. In particular, when is it better to think in terms of localized closed-shell singlets and when is it better to think in terms of delocalized open-shell singlets (i.e., a little like in Figs. 3 and 4)?

## Acknowledgements

AJE, OM, and MEC met through the African School of Electronic Structure Methods and Applications (ASESMA) and are grateful for the learning and networking possibilities provided by ASESMA. MEC been involved in the deMon developers group from the time of its creation. MEC is grateful to Pierre Girard for configuring the personal computer on which some of the calculations reported here were performed.

## Supplementary Information

The following supplementary information associated with this article is available on-line:

1. Digitized reference potential energy curves
2. Group theoretic analysis
3. Sample DEMON2K input
4. Multiplet sum method potential energy curves
5. Tables comparing calculated and experimental atomic and diatomic calculated parameters
6. Author contributions

## References

- [1] D. R. Kearns, [Physical and chemical properties of singlet molecular oxygen](#), Chem. Rev. **71**, 395 (1971).
- [2] S. W. Ryter and R. M. Tyrrell, [Singlet molecular oxygen \( \$^1\text{O}\_2\$ \): A possible effector of eukaryotic gene expression](#), Free Radical Biol. Med. **24**, 1520 (1998).
- [3] M. C. DeRosa and R. J. Crutchley, [Photosensitized singlet oxygen and its application](#), Coord. Chem. Rev. **233-234**, 351 (2002).
- [4] M. J. Paterson, O. Christiansen, F. Jensen, and P. R. Ogilby, [Overview of theoretical and computational methods applied to the oxygen-organic molecule photosystem](#), Photochem. Photobiol. **82**, 1136 (2006).
- [5] P. R. Ogilby, [Singlet oxygen: there is indeed something new under the sun](#), Chem. Soc. Rev. **39**, 3181 (2010).
- [6] T. Ziegler, A. Rauk, and E. J. Baerends, [On the calculation of multiplet energies by the Hartree-Fock-Slater method](#), Theor. Chim. Acta **4**, 877 (1977).

- [7] C. Daul, [Density functional theory applied to the excited states of coordination compounds](#), *Int. J. Quantum Chem.* **52**, 867 (1994).
- [8] A. Lavoisier, *Traité élémentaire de Chimie, présenté dans un ordre nouveau et d'après les découvertes modernes*, Chez Cuchet, Paris, 1789.
- [9] W. T. Borden, R. Hoffmann, T. Stuyver, and B. Chen, [Dioxygen: What makes this triplet diradical kinetically persistent?](#), *J. Am. Chem. Soc.* **139**, 9010 (2017).
- [10] A. J. Etindele, R. Maezono, R. L. M. Melono, and O. Motapon, [Influence of endohedral confinement of atoms on structural and dynamical properties of the C<sub>60</sub> fullerene](#), *Chem. Phys. Lett.* **685**, 395 (2017).
- [11] A. A. M. H. M. Darghouth, M. E. Casida, X. Zhu, B. Natarajan, H. Su, A. Humeniuk, and R. Mitrić, [Effect of varying the TD-Ic-DFTB range-separation parameter on charge and energy transfer in a model pentacene/buckminsterfullerene heterojunction](#), *J. Chem. Phys.* **154**, 054102 (2021).
- [12] L. Brunet, D. Y. Lyon, E. M. Hotze, P. J. J. Alvarez, and M. R. Wiesner, [Comparative photoactivity and antibacterial properties of C<sub>60</sub> fullerenes and titanium dioxide nanoparticles](#), *Environ. Sci. Technol.* **43**, 4355 (2009).
- [13] M. R. Hamblin, [Fullerenes as photosensitizers in photodynamic therapy: pros and cons](#), *Photochem. Photobiol. Sci.* **17**, 1515 (2018).
- [14] Y. Yamakoshi, N. Umezawa, A. Ryu, K. Arakane, N. Miyata, Y. Goda, T. Masumizu, and T. Nagano, [Active oxygen species generated from photoexcited fullerene \(C<sub>60</sub>\) as potential medicines: O<sub>2</sub><sup>•-</sup> versus <sup>1</sup>O<sub>2</sub>](#), *J. Am. Chem. Soc.* **125**, 12803 (2003).
- [15] H. Fueno, Y. Takenaka, and K. Tanaka, [Theoretical study on energy transfer from the excited C<sub>60</sub> to molecular oxygen](#), *Opt. Spectrosc.* **111.2**, 248 (2011).
- [16] M. Garavelli, F. Bernardi, M. Olivucci, and M. A. Robb, [DFT study of the reactions between singlet-oxygen and a carotenoid model](#), *J. Am. Chem. Soc.* **120**, 10210 (1998).
- [17] J. Al-Nu'airat, M. Altarawneh, X. Gao, P. R. Westmoreland, and B. Z. Dlugogorski, [Reaction of aniline with singlet oxygen \(O<sub>2</sub><sup>1</sup>δ<sub>g</sub>\)](#), *J. Phys. Chem. A* **121**, 17 (2017).
- [18] [National institute of standards and technologies computational chemistry comparison and benchmark data base](#), <https://cccbdb.nist.gov/stgap3x.asp?im=90&ib=32&estate1=4&estate2=1>, Last accessed 16 July 2021.
- [19] Z. Zu, [Reactivities of singlet oxygen: open-shell or closed-shell?](#), *Phys. Chem. Chem. Phys.* **22**, 13373 (2020).
- [20] Z. Farooq, D. A. Chestakov, B. Yan, G. C. Groenenboom, W. J. van der Zande, and D. H. Parker, [Photodissociation of singlet oxygen in the UV region](#), *Phys. Chem. Chem. Phys.* **16**, 3305.
- [21] K. Yamaguchi, F. Jensen, A. Dorigo, and K. Houk, [A spin correction procedure for unrestricted Hartree-Fock and Möller-Plesset wavefunctions for singlet diradicals and polyradicals](#), *Chem. Phys. Lett.* **149**, 537 (1988).

- [22] S. Yamanaka, T. Kawakami, H. Nagao, and K. Yamaguchi, [Effective exchange integrals for open-shell species by density functional methods](#), Chem. Phys. Lett. **231**, 25 (1994).
- [23] J. M. Wittbrodt and M. B. J. Schlegel, [Some reasons not to use spin projected density functional theory](#), Chem. Phys. **105**, 6574 (1996).
- [24] G. Geudtner, P. Calaminici, J. Carmona-Espindola, J. M. del Campo, V. D. Dominguez-Soria, R. Flores-Moreno, G. U. Gamboa, A. Goursot, A. M. Kster, J. U. Reveles, T. Mineva, J. M. Vasquez-Perez, A. Vela, B. Zuñiga-Gutierrez, and D. Salahub, [DEMON2K](#), WIREs: Comput. Mol. Sci. **2**, 548 (2012).
- [25] A. Rohatgi, [WEBPLOTDIGITIZER: Webbased plot digitizer](#), <https://apps.automeris.io/wpd/>, Last accessed 3 June 2021.
- [26] P. H. Krupenie, [The spectrum of molecular oxygen](#), J. Phys. Chem. Ref. Data **1**, 423 (1972).
- [27] R. P. Saxon and B. Liu, [Ab initio configuration interaction study of the valence states of O<sub>2</sub>](#), J. Chem. Phys. **67** (1977).
- [28] M. C. G. N. van Vroonhoven and G. C. Groenenboom, [Reassignment of the O<sub>2</sub> spectrum just below dissociation threshold based on ab initio calculations](#), J. Chem. Phys. **117**, 5240 (2002).
- [29] M. Laing, [The three forms of molecular oxygen](#), J. Chem. Ed. **66**, 453 (1989).
- [30] Wikipedia, [Singlet oxygen](#), [https://en.wikipedia.org/wiki/Singlet\\_oxygen](https://en.wikipedia.org/wiki/Singlet_oxygen), Last accessed 24 June 2021.
- [31] T. S. Carlton, [Why the lower-energy term of singlet dioxygen has a doubly occupied  \$\pi^\*\$  orbital](#), J. Chem. Ed. **83**, 477 (2006).
- [32] [National institute of standards and technologies atomic spectra database](#), [https://physics.nist.gov/PhysRefData/ASD/levels\\_form.html](https://physics.nist.gov/PhysRefData/ASD/levels_form.html), Last accessed 22 June 2021.
- [33] K. E. Hyde, [Methods for obtaining Russell-Saunders term symbols from electronic configurations](#), J. Chem. Ed. **52**, 87 (1975).
- [34] T. Stuyver, B. Chen, T. Zeng, P. Geerlings, F. D. Proft, and R. Hoffmann, [Do diradicals behave like radicals?](#), Chem. Rev. **119**, 11291 (2019).
- [35] L. Noodleman, [Valence bond description of antiferromagnetic coupling in transition metal dimers](#), J. Chem. Phys. **74**, 5737 (1981).
- [36] J. Friedrichs and I. Frank, [Mechanism of electrocyclic ring-opening of diphenyloxirane: 40 years after Woodward and Hoffmann](#), Chemistry — A European Journal **15**, 10825 (2009).
- [37] M. E. Casida and M. Huix-Rotllant, [Progress in time-dependent density-functional theory](#), Annu. Rev. Phys. Chem. **63**, 287 (2012).
- [38] A. M. Koster et al., [DEMON2K: density of Montreal, version 5.0](#), The deMon developers, Cinvestav, Mexico City (2018), [http://www.demon-software.com/public\\_html/index.html](http://www.demon-software.com/public_html/index.html), Last accessed 3 July 2021.

- [39] A. de la Lande, A. Alvarez-Ibarra, K. Hasnaoui, F. Cailliez, X. Wu, T. Mineva, J. Cuny, P. Calaminici, L. López-Sosa, G. Geudtner, I. Navizet, C. Garcia Iriepa, D. R. Salahub, and A. M. Köster, [Molecular simulations with in DEMON2K QM-MM, a tutorial-review](#), *Molecules* **24** (1653).
- [40] P. Löwdin, [Quantum theory of many-particle systems. II. Study of the ordinary Hartree-Fock approximation](#), *Phys. Rev.* **97**, 1490 (1955).
- [41] H. Myneni and M. E. Casida, [On the calculation of  \$\delta\langle\hat{S}^2\rangle\$  for electronic excitations in time-dependent density-functional theory](#), *Comput. Phys. Comm.* **213**, 72 (2017).
- [42] J. P. Perdew and K. Schmidt, [Jacob's ladder of density functional approximations for the exchange-correlation energy](#), in *Density Functional Theory and its Applications to Materials*, edited by V. E. V. Doren, K. V. Alseoy, and P. Geerlings, page 1, American Institute of Physics, Melville, New York, 2001.
- [43] J. P. Perdew, A. Ruzsinsky, L. A. Constantin, J. Sun, and G. Csonka, [Some fundamental issues in ground-state density functional theory: a guide for the perplexed](#), *J. Chem. Theor. Comput.* **5**, 902 (2009).
- [44] L. Goerigk and N. Mehta, [A trip to the density functional theory zoo: Warnings and recommendations for the user](#), *Aust. J. Chem.* **72**, 563 (2019).
- [45] D. P. O'Neill and P. M. W. Gill, [Benchmark correlation energies for small molecules](#), *Mol. Phys.* **103**, 763 (2005).
- [46] Y. Zhao and D. G. Truhlar, [The M06 suite of density functionals for main group thermochemistry, thermochemical kinetics, noncovalent interactions, excited states, and transition elements: two new functionals and systematic testing of four M06-class functionals and 12 other functionals](#), *Theor. Chem. Acc.* **120**, 215 (2007).
- [47] A. Fouqueau, S. Mer, M. E. Casida, L. M. L. Daku, A. Hauser, T. Mineva, and F. Neese, [Comparison of density functionals for energy and structural differences between the high \[ \${}^5T\_{2g} : \(t\_{2g}\)^4\(e\_g\)^2\$ \] and low \[ \${}^1A\_{1g} : \(t\_{2g}\)^6\(e\_g\)^0\$ \] spin states of the hexaquoferrous cation,  \$\[\text{Fe}\(\text{H}\_2\text{O}\)\_6\]^{2+}\$](#) , *J. Chem. Phys.* **120**, 9473 (2004).
- [48] A. Fouqueau, M. E. Casida, L. M. L. Daku, A. Hauser, and F. Neese, [Comparison of density functionals for energy and structural differences between the high \[ \${}^5T\_{2g} : \(t\_{2g}\)^4\(e\_g\)^2\$ \] and low \[ \${}^1A\_{1g} : \(t\_{2g}\)^6\(e\_g\)^0\$ \] spin states of iron\(II\) coordination compounds: II. More functionals and the hexaminoferrous cation,  \$\[\text{Fe}\(\text{NH}\_3\)\_6\]^{2+}\$](#) , *J. Chem. Phys.* **122**, 044110 (2005).
- [49] G. Ganzenmüller, N. Berkaine, A. Fouqueau, M. E. Casida, and M. Reiher, [Comparison of density functionals for differences between the high \( \${}^5T\_{2g}\$ \) and low \( \${}^1A\_{1g}\$ \) spin states of iron\(II\) coordination compounds: IV. Results for the ferrous complexes  \$\[\text{Fe}\(\text{L}\)\(\text{'NHS}\_4\text{'}\)\]\$](#) , *J. Chem. Phys.* **122**, 234321 (2005).
- [50] L. M. L. Daku, A. Vargas, A. Hauser, A. Fouqueau, and M. E. Casida, [Assessment of density functionals for the high-spin/low-spin energy difference in the low-spin iron\(II\) tris\(2,2'-bipyridine\) complex](#), *ChemPhysChem* **6**, 1393 (2005).

- [51] S. Zein, S. A. Borshch, P. Fleurat-Lessard, M. E. Casida, and H. Chermette, [Assessment of the exchange-correlation functionals for the physical description of spin transition phenomena by DFT methods: All the same?](#), *J. Chem. Phys.* **126**, 014105 (2007).
- [52] S. Song, M. Kim, E. Sim, A. Benali, O. Heinonen, and K. Burke, [Benchmarks and reliable DFT results for spin gaps of small ligand Fe\(II\) complexes](#), *J. Chem. Theory Comput.* **14**, 2304 (2018).
- [53] P. M. Morse, [Diatomic molecules according to the wave mechanics. II. Vibrational levels](#), *Phys. Rev.* **34**, 57 (1929).
- [54] P. Hohenberg and W. Kohn, [Inhomogeneous electron gas](#), *Phys. Rev.* **136**, B864 (1964).
- [55] W. Kohn and L. J. Sham, [Self-consistent equations including exchange and correlation effects](#), *Phys. Rev.* **140**, A1133 (1965).
- [56] M. E. Casida, [Generalization of the optimized effective potential model to include electron correlation: A variational derivation of the Sham–Schluter equation for the exact exchange-correlation potential](#), *Phys. Rev. A* **51**, 2005 (1995).
- [57] M. E. Casida, [Review: Time-dependent density-functional theory for molecules and molecular solids](#), *J. Mol. Struct. (Theochem)* **914**, 3 (2009).
- [58] M. E. Casida, [Reconciling of the  \$\Delta\$ SCF and TDDFT approaches to excitation energies in DFT: A charge-transfer correction for TDDFT with GGA functionals](#), *On-line Workshop Proceedings of the Joint ITP/INT Workshop on Time-Dependent Density Functional Theory*, 15-17 April 1999, Institute for Theoretical Physics, University of California at Santa Barbara: [http://www.itp.ucsb.edu/online/tddft\\_c99/](http://www.itp.ucsb.edu/online/tddft_c99/), Last accessed 25 July 2021.
- [59] M. E. Casida, F. Gutierrez, J. Guan, F. Gadea, D. R. Salahub, and J. Daudey, [Charge-transfer correction for improved time-dependent local density approximation excited-state potential energy curves: Analysis within the two-level model with illustration for H<sub>2</sub> and LiH](#), *J. Chem. Phys.* **113**, 7062 (2000).
- [60] T. Ziegler, M. Seth, M. Krykunov, J. Autschbach, and F. Wang, [On the relation between time-dependent and variational density functional theory approaches for the determination of excitation energies and transition moments](#), *J. Chem. Phys.* **130**, 154102 (2009).
- [61] T. Ziegler, M. Krykunov, and J. Cullen, [The implementation of a self-consistent constricted variational density functional theory for the description of excited states](#), *J. Chem. Phys.* **136**, 124107 (2012).
- [62] S. Hirata and M. Head-Gordon, [Time-dependent density functional theory within the Tamm-Dancoff approximation](#), *Chem. Phys. Lett.* **314**, 291 (1999).
- [63] J. Guan, M. E. Casida, and D. R. Salahub, [Time-dependent density-functional theory investigation of excitation spectra of open-shell molecules](#), *J. Molec. Structure (Theochem)* **527**, 229 (2000).
- [64] M. E. Casida, A. Ipatov, and F. Cordova, [Linear-response time-dependent density-functional theory for open-shell molecules](#), in *Time-Dependent Density-Functional Theory*, edited by M. A. L. Marques, C. Ullrich, F. Nogueira, A. Rubio, and E. K. U. Gross, page 243, Springer, Berlin, 2006, Lecture Notes in Physics.

- [65] A. Ipatov, F. Cordova, L. Joubert Doriol, and M. E. Casida, [Excited-state spin-contamination in time-dependent density-functional theory for molecules with open-shell ground states](#), *J. Mol. Struct. (Theochem)* **914**, 60 (2009).
- [66] L. V. Slipchenko and A. I. Krylov, [Electronic structure of the trimethylenemethane diradical in its ground and electronically excited states: Bonding, equilibrium geometries, and vibrational frequencies](#), *J. Chem. Phys.* **118**, 6874 (2003).
- [67] Y. Shao, M. Head-Gordon, and A. I. Krylov, [The spin-flip approach within time-dependent density functional theory: Theory and applications to diradicals](#), *J. Chem. Phys.* **118**, 4807 (2003).
- [68] F. Wang and T. Ziegler, [Time-dependent density functional theory based on a noncollinear formulation of the exchange-correlation potential](#), *J. Chem. Phys.* **121**, 12191 (2004).
- [69] F. Wang and T. Ziegler, [Use of noncollinear exchange-correlation potentials in multiplet resolutions by time-dependent density functional theory](#), *Int. J. Quantum Chem.* **106**, 2545 (2006).
- [70] N. Minezawa and M. S. Gordon, [Optimizing conical intersections by spin-flip density functional theory: application to ethylene](#), *J. Phys. Chem. A* **113**, 12749 (2009).
- [71] M. Huix-Rotllant, B. Natarajan, A. Ipatov, C. M. Wawire, T. Deutsch, and M. E. Casida, [Assessment of noncollinear spin-flip Tamm-Dancoff approximation time-dependent density-functional theory for the photochemical ring-opening of oxirane](#), *Phys. Chem. Chem. Phys.* **12**, 12811 (2010).
- [72] R. J. Cave, F. Zhang, N. T. Maitra, and K. Burke, [A dressed TDDFT treatment of the  \$2^1A\_g\$  states of butadiene and hexatriene](#), *Chem. Phys. Lett.* **389**, 39 (2004).
- [73] N. T. Maitra, F. Zhang, R. J. Cave, and K. Burke, [Double excitations within time-dependent density functional theory linear response](#), *J. Chem. Phys.* **120**, 5932 (2004).
- [74] M. E. Casida, [Propagator corrections to adiabatic time-dependent density-functional theory linear response theory](#), *J. Chem. Phys.* **122**, 054111 (2005).
- [75] M. Huix-Rotllant, A. Ipatov, A. Rubio, and M. E. Casida, [Assessment of dressed time-dependent density-functional theory for the low-lying valence states of 28 organic chromophores](#), *Chem. Phys.* **391**, 120 (2011).
- [76] M. E. Casida and M. Huix-Rotllant, [Many-body perturbation theory \(MBPT\) and time-dependent density-functional theory \(TD-DFT\): MBPT insights about what is missing in, and corrections to, the TD-DFT adiabatic approximation](#), in *Topics in Current Chemistry, special volume on Density-Functional Methods for Excited States*, edited by N. Ferré, M. Filatov, and M. Huix-Rotllant, Springer, 2015.
- [77] J. Guan, F. Wang, T. Ziegler, and H. Cox, [Time-dependent density functional study of the electronic potential energy curves and excitation spectrum of the oxygen molecule](#), *J. Chem. Phys.* **125**, 044314 (2006).
- [78] A. Cembran, L. C. Song, Y. R. Mo, and J. Gao, [Block-localized density functional theory \(BLDFT\), diabatic coupling, and their use in valence bond theory for representing reactive potential energy surfaces](#), *J. Chem. Theory Comput.* **5**, 2702 (2009).

- [79] H. S. Ren, M. R. Provorse, P. Bao, Z. X. Qu, and J. Gao, [Multistate density functional theory for effective diabatic electronic coupling](#), *J. Phys. Chem. Lett.* **7**, 2286 (2016).
- [80] A. Grofe, X. Chen, W. Liu, and J. Gao, [Spin-multiplet components and energy splittings by multistate density functional theory](#), *J. Phys. Chem. Lett.* **8**, 4838 (2017).
- [81] A. Grofe, Z. X. Qu, D. G. Truhlar, H. Li, and J. Gao, [Diabatic-at-construction method for diabatic and adiabatic ground and excited states based on multistate density functional theory](#), *J. Chem. Theory Comput.* **13**, 1176 (2017).
- [82] L. Yang, A. Grofe, J. Reimers, and J. Gao, [Multistate density functional theory applied with 3 unpaired electrons in 3 orbitals: the singdoublet and tripdoublet states of the ethylene cation](#), *Chem. Phys. Lett.* **736**, 136803 (2019).
- [83] Q. Wu and T. V. Voorhis, [Constrained density functional theory and its application in long-range electron transfer](#), *J. Chem. Theory Comput.* **2**, 765 (2006).
- [84] Q. Wu, C. L. Cheng, and T. V. Voorhis, [Configuration interaction based on constrained density functional theory: A multireference method](#), *J. Chem. Phys.* **127**, 164119 (2007).
- [85] B. Kaduk and T. V. Voorhis, [Communication: Conical intersections using constrained density functional theory-configuration interaction](#), *J. Chem. Phys.* **133**, 061102 (2010).
- [86] B. Kaduk, T. Kowalczyk, and T. V. Voorhis, [Constrained density functional theory](#), *Chem. Rev.* **112**, 321 (2012).
- [87] M. G. Mavros and T. V. Voorhis, [Communication: CDFT-CI couplings can be unreliable when there is fractional charge transfer](#), *J. Chem. Phys.* **143**, 231102 (2015).
- [88] A. de la Lande and D. R. Salahub, [Derivation of interpretive models for long range electron transfer from constrained density functional theory](#), *J. Mol. Struct. (THEOCHEM)* **943**, 115 (2010).
- [89] R. Řezáč, B. Lévy, I. Demachy, and A. de la Lande, [Robust and efficient constrained DFT molecular dynamics approach to biochemical modeling](#), *J. Chem. Theory Comput.* **8**, 418 (2012).